(Fig. 2c). Moreover, the glucose-lowering effect of insulin was decreased in *Angptl6*$^{-/-}$ mice relative to controls, indicating insulin resistance in *Angptl6*$^{-/-}$ mice (**Fig. 2d**). Recent studies have shown a role for tumor necrosis factor (TNF)-α[18,19] secreted from adipose tissue as a mediator of insulin resistance, and adiponectin[20,21] and leptin[22,23] have a role in insulin sensitivity. The leptin concentration in *Angptl6*$^{-/-}$ mice was significantly higher than that seen in controls, whereas no significant differences were observed in adiponectin and TNF-α concentrations between genotypes (**Fig. 2e**).

Molecular alterations in *Angptl6*$^{-/-}$ mice

The physiological data presented above indicate that inactivation of AGF *in vivo* leads to decreased energy expenditure and obesity. Recent studies indicate that BAT and skeletal muscle function as tissues mediating adaptive thermogenesis, which is an important defense against obesity[24,25]. To determine the molecular basis of these metabolic changes in *Angptl6*$^{-/-}$ mice, we examined the expression of molecules with proposed roles in obesity and associated metabolic action in BAT and skeletal muscle. Quantitative RT-PCR analysis showed significant decreases in expression of PPARα, PPARγ, PGC-1β and UCP1 in BAT (**Fig. 2f**) and PPARδ and UCP3 in skeletal muscle (**Fig. 2g**) in *Angptl6*$^{-/-}$ mice, suggesting that such alterations in gene expression underlie susceptibility to obesity in *Angptl6*$^{-/-}$ mice.

Generation of *Angptl6*-transgenic mice

Observations that AGF ablation causes obesity prompted us to further investigate whether AGF functions in resistance to obesity and associated disorders. To generate mice overexpressing AGF constitutively, we targeted the activation of *Angptl6 in vivo* by driving its expression from the chicken β-actin promoter with the cytomegalovirus immediate-early enhancer (CAG promoter)[26,27] (**Supplementary Fig. 2** online). The CAG promoter has been reported to be strongly active in a variety of tissues. In our mice, the promoter drove high expression of the *Angptl6* transgene in BAT, heart and skeletal muscle relative to expression of the endogenous gene in each tissue (**Supplementary Fig. 2**). AGF concentration in the circulation of *Angptl6* transgenic mice increased approximately twofold compared with basal concentrations in nontransgenic controls (**Fig. 3a**).

Leanness in *Angptl6* transgenic mice

Despite a daily food intake similar to that of controls when individually housed and fed a normal chow diet (transgenic mice, 0.17 ± 0.05

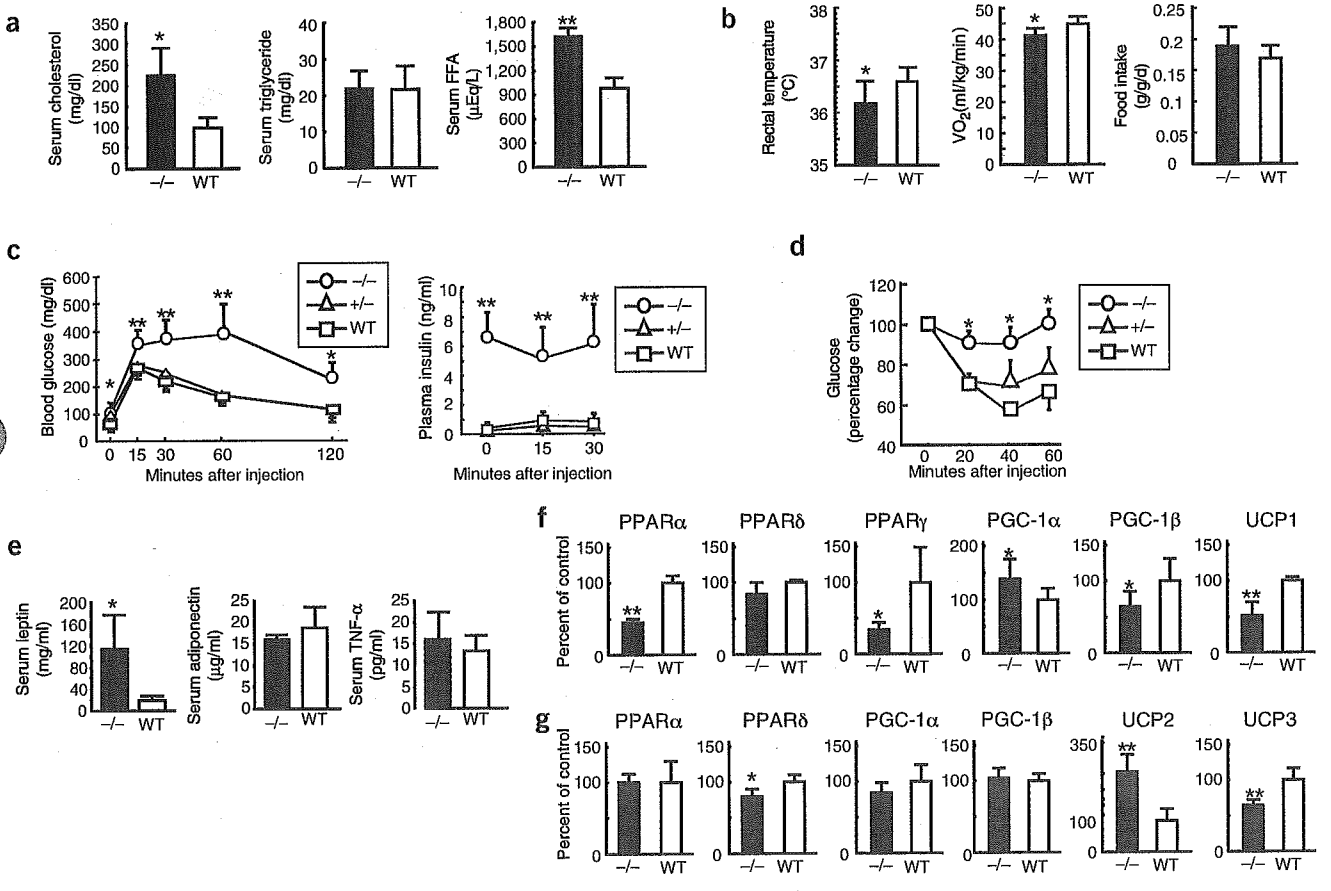

Figure 2 Metabolic effects of AGF deficiency on a normal diet. (**a**) Serum cholesterol, triglyceride and FFA concentrations in *Angptl6*$^{-/-}$ and wild-type control mice at 5 months of age ($n = 5$ in each group). (**b**) Rectal temperature, oxygen consumption (VO_2)/lean body weight and food intake/lean body weight in *Angptl6*$^{-/-}$ and wild-type mice at 6 months of age ($n = 8$ in each group). (**c**,**d**) Glucose (**c**) and insulin (**d**) tolerance tests in *Angptl6*$^{-/-}$, *Angptl6*$^{+/-}$ and wild-type mice at 3 months of age ($n = 6$ in each group). (**e**) Serum leptin, adiponectin, and TNF-α concentrations in *Angptl6*$^{-/-}$ and wild-type mice at 5 months of age ($n = 5$ in each group). (**f**,**g**) Expression of genes associated with energy expenditure in BAT (**f**) and skeletal muscle (**g**) of *Angptl6*$^{-/-}$ relative to wild-type mice (100%) at 3 months of age ($n = 5$ in each group). Data are mean ± s.d. $^*P < 0.05$, $^{**}P < 0.01$, between the two genotypes indicated or among three genotypes. Female mice were used for all experiments.

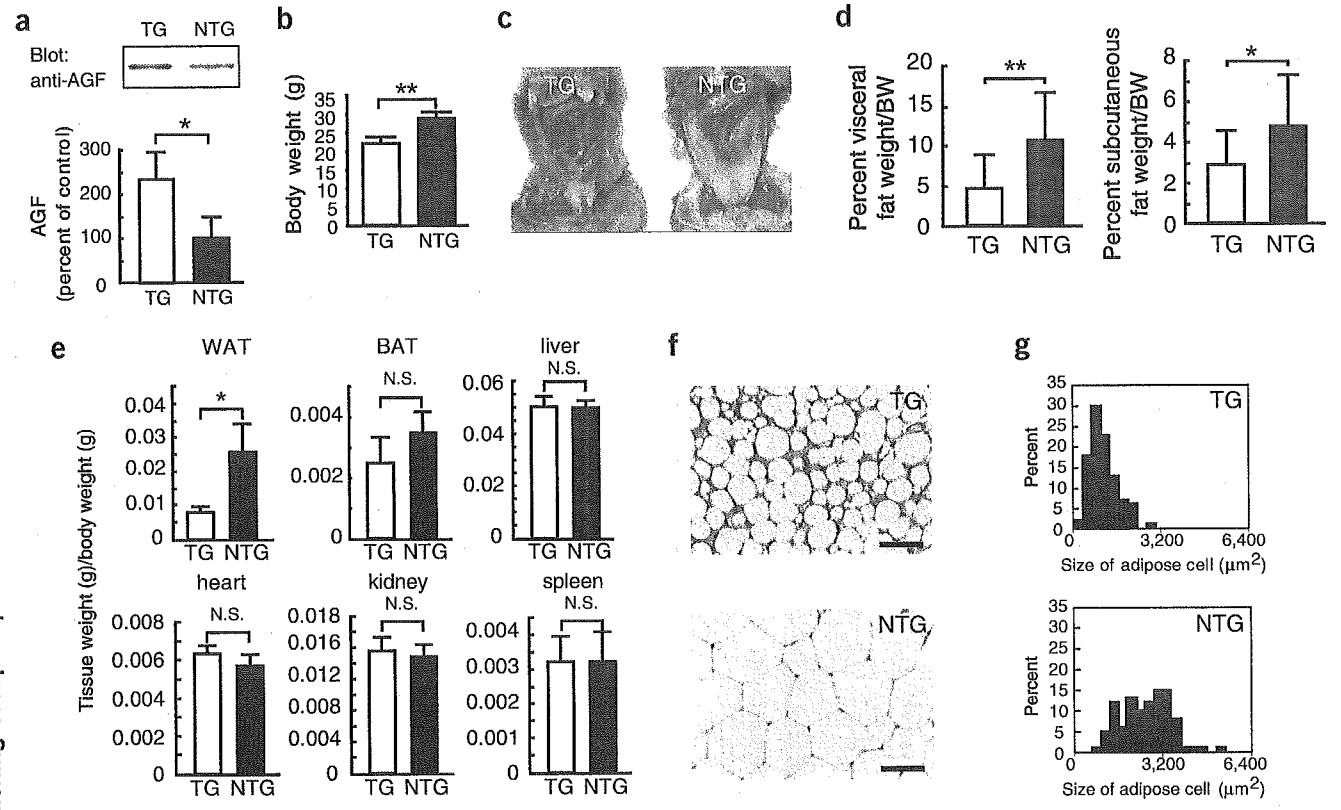

Figure 3 *Angptl6* transgenic mice are lean as a result of a loss of WAT mass. (**a**) Western blotting analysis for serum AGF in *Angptl6* transgenic (TG) and nontransgenic control (NTG) mice at 4 months of age. The ratio for the control is set as 100%. (**b–g**) Body weight (**b**), and gross appearance of visceral adipocyte (**c**) in TG and NTG mice at 4 months of age. (**d**) Comparison of visceral fat and subcutaneous fat weight/body weight between TG and NTG mice at 5 months of age. Tissue weight/body weight in TG and NTG mice at 4 months of age (**e**). $n = 10–15$ in each group. Histological analysis (**f**) and distribution of cell size (**g**) of WAT from TG and NTG mice at 4 months of age. Scale bars, 50 μm. Data are mean ± s.d. $^*P < 0.05$, $^{**}P < 0.01$, between the two genotypes indicated. N.S. indicates no significant difference compared with nontransgenic wild-type mice. Female mice were used for all experiments.

versus control mice, 0.15 ± 0.03 g/g lean body mass/d), 5-month-old *Angptl6* transgenic mice showed marked reductions in body weight and adiposity compared with controls (**Fig. 3b–d**). Although there was no alteration in body weight at birth between genotypes, a reduction in body weight of *Angptl6* transgenic mice compared to controls was noted 4 weeks after birth and persisted throughout their life. There were no differences of this alteration in body weight between male and female mice. Furthermore, only WAT weight per body weight in *Angptl6* transgenic mice was markedly decreased compared to that of controls (**Fig. 3e**). Adipocytes from *Angptl6* transgenic mice are smaller in size compared to those from controls, indicating that a reduction in total fat mass may result from decreased triglyceride accumulation (**Fig. 3f,g**).

Metabolic alterations in *Angptl6* transgenic mice

There was no difference in *in vitro* adipocyte differentiation of embryonic fibroblasts between *Angptl6* transgenic mice and controls (data not shown). To address alternative causes for decreased adiposity in *Angptl6* transgenic mice, we compared rectal temperature and basal metabolic rates of *Angptl6* transgenic mice and controls. Transgenic mice showed a small, statistically insignificant increase in rectal temperature and a statistically significant increase in whole-body oxygen consumption rates relative to controls (**Fig. 4a**), suggesting the enhanced energy expenditure in *Angptl6* transgenic mice. The microvasculature assists in heat dissipation at sites of active thermogenesis, increasing the efficiency of lipid release from fat stores[28,29]. *Angptl6* transgenic mice showed an increase in the number of capillary-sized vessels in skeletal muscles compared to controls (**Fig. 4b**), suggesting that AGF assists in part to increase thermogenesis in *Angptl6* transgenic mice.

Quantitative RT-PCR analysis showed significant increases in expression of the genes encoding PPARα, PPARγ and PGC-1β in BAT (**Fig. 4c**) and of the genes encoding PPARα, PPARδ, PGC-1α and UCP2 in skeletal muscle (**Fig. 4d**) in *Angptl6* transgenic mice. These findings suggest that overexpression of AGF *in vivo* activates molecules involved in stimulating energy expenditure, and thereby leads to decreased adiposity.

Insulin sensitivity in *Angptl6* transgenic mice

A lack of fat causes decreases in serum levels of leptin and adiponectin and leads to insulin resistance and diabetes[21,22,30,31]. Although *Angptl6* transgenic mice showed decreased serum leptin levels, identical serum adiponectin levels were observed in transgenic and wild-type mice (**Fig. 4e**). Serum adiponectin levels per WAT mass in *Angptl6* transgenic mice were markedly increased compared with that of wild-type mice, whereas there was no difference in serum leptin levels per WAT mass (**Fig. 4e**), suggesting that adipose tissues in *Angptl6* transgenic mice secrete adiponectin abundantly. Notably, IGTT and ITT showed that *Angptl6* transgenic mice show increased insulin sensitivity despite the greatly decreased serum leptin and identical serum adiponectin levels

(**Fig. 4f,g**), suggesting that increased insulin sensitivity observed in *Angptl6* transgenic mice depends on direct effects of increased serum AGF.

Resistance to obesity in *Angptl6*-transgenic mice

To investigate whether *Angptl6* transgenic mice show resistance against developing obesity, we challenged 8-week-old female mice with a high-fat diet containing 32% (wt/wt) fat for 12 weeks to stimulate weight gain. *Angptl6* transgenic mice fed this diet showed significant differences from controls: at the end of the feeding period, the net weight gains were 7.13 ± 1.03 g and 21.86 ± 4.03 g, respectively, for *Angptl6* transgenic and controls (**Fig. 5a,b**). As expected, high-fat feeding causes massive lipid accumulation in both visceral and subcutaneous fat depots in controls, whereas few of these changes are seen in *Angptl6* transgenic mice (**Fig. 5c,d**). Notably, the size of WAT from *Angptl6* transgenic mice was markedly smaller than that of WAT from controls (**Fig. 5e**). No appreciable fatty acid accumulation in BAT, liver and skeletal muscle was observed in *Angptl6* transgenic mice, whereas nontransgenic mice develop tissue steatosis (**Fig. 5e,f**). There was no significant difference in blood glucose levels between genotypes (**Fig. 5g**). But plasma insulin levels in *Angptl6* transgenic mice were much lower than those seen in controls (**Fig. 5g**). Whereas high-fat feeding increases serum cholesterol and FFA levels by twofold in controls, *Angptl6* transgenic mice showed a lipid profile closer to that of wild-type mice fed a standard chow diet (**Fig. 5g**).

AGF antagonizes obesity and insulin resistance

To clarify whether AGF decreases body weight and insulin resistance of obese mice, we intravenously injected adenovirus expressing mouse AGF (Ad-AGF) into female mice fed a high-fat diet containing 32% (wt/wt) fat for 12 months. For controls, adenovirus expressing green fluorescent protein (GFP) (Ad-GFP) was injected. There was no significant difference in body weight between the mice with AGF treatment and controls (54.4 ± 2.2 g and 52.9 ± 2.1 g, respectively: $P = 0.18$, $n = 8$). Throughout the time course of the experiment, mice continued to receive a high-fat diet. On day 20, mice receiving AGF showed approximately 2.5-fold increases in serum AGF levels compared to controls (**Fig. 6a**), and showed significant loss of body weight compared to controls (**Fig. 6b**). No significant difference between the two groups was observed in daily food intake (**Fig. 6c**). Furthermore, significant decreases in fasting and random fed glucose levels were observed in high-fat diet–induced obese mice after treatment with AGF compared to those in controls (**Fig. 6d,e**). IGTT and IITT showed that high-fat diet–induced obese mice with AGF treatment showed improved glucose tolerance and increased insulin sensitivity (**Fig. 6f,g**). Taken together, these data clearly show that AGF counteracts obesity and related insulin resistance.

DISCUSSION

AGF, a member of the Angptl family, is a circulating angiogenic protein secreted by liver[7]. Here, we show that most (>80%) of the AGF-deficient mice die at approximately embryonic day 13, with apparent cardiovascular defects including poorly formed yolk sac and vitelline vessels. Notably, the surviving *Angptl6*$^{-/-}$ mice become markedly obese and show obesity-related metabolic disorders. Furthermore, *Angptl6*$^{-/-}$ mice show decreased whole-body oxygen consumption and expression of genes involved in energy dissipation. In parallel, *Angptl6* transgenic mice show resistance against diet-induced obesity, insulin resistance and hyperlipidemia. These phenotypes are associated with increases in energy expenditure, supporting the hypothesis that AGF regulates energy metabolism in mice.

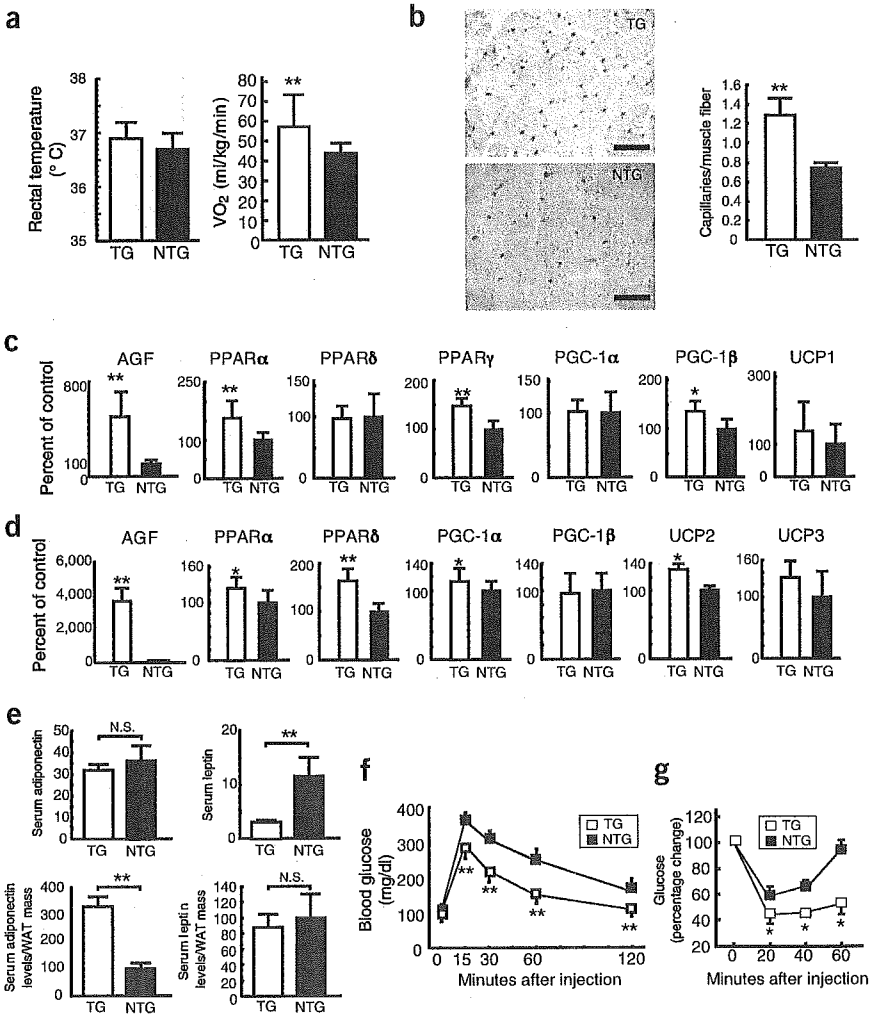

Figure 4 Metabolic and vascular alteration in *Angptl6* transgenic mice. (**a**) Rectal temperature and oxygen consumption (VO_2)/lean body weight in *Angptl6* transgenic (TG) and nontransgenic (NTG) female mice at 5 months of age (n = 10–12 in each group; these mice were also used in **Fig. 4e,f**). (**b**) Representative photograph of CD31/PECAM-1-stained capillary vessels and quantitative estimation of capillary vessel density in the gastrocnemius muscle in TG and NTG female mice at 4 months of age. Scale bars, 50 μm. (**c,d**) Relative ratio of gene expression associated with increased energy expenditure in BAT (**c**) and skeletal muscle (**d**) in TG mice relative to that seen in NTG female and male mice at 4 months of age. The ratio for the data from NTG mice is set as 100%. (**e**) Serum adiponectin and leptin levels and serum adiponectin and leptin levels/ WAT mass in TG and NTG female mice at 4 months of age. (**f,g**) Glucose (**f**) and insulin (**g**) tolerance tests in TG and NTG female mice at 4 months of age. Data are mean ± s.d. (n = 5–15). *P < 0.05, **P < 0.01, between the two genotypes indicated. N.S. indicates no significant difference compared with NTG mice.

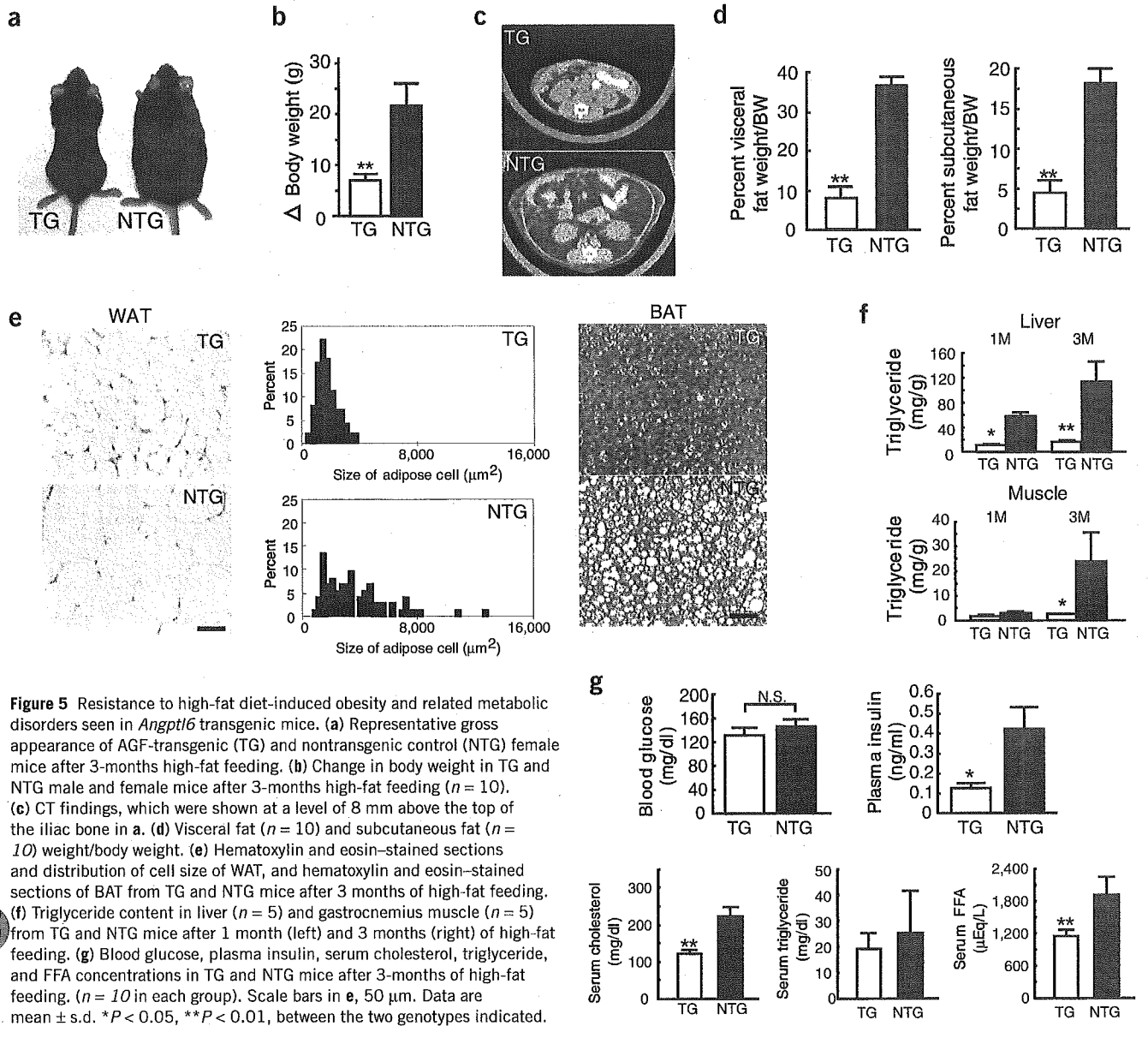

Figure 5 Resistance to high-fat diet-induced obesity and related metabolic disorders seen in *Angptl6* transgenic mice. (**a**) Representative gross appearance of AGF-transgenic (TG) and nontransgenic control (NTG) female mice after 3-months high-fat feeding. (**b**) Change in body weight in TG and NTG male and female mice after 3-months high-fat feeding ($n = 10$). (**c**) CT findings, which were shown at a level of 8 mm above the top of the iliac bone in **a**. (**d**) Visceral fat ($n = 10$) and subcutaneous fat ($n = 10$) weight/body weight. (**e**) Hematoxylin and eosin–stained sections and distribution of cell size of WAT, and hematoxylin and eosin–stained sections of BAT from TG and NTG mice after 3 months of high-fat feeding. (**f**) Triglyceride content in liver ($n = 5$) and gastrocnemius muscle ($n = 5$) from TG and NTG mice after 1 month (left) and 3 months (right) of high-fat feeding. (**g**) Blood glucose, plasma insulin, serum cholesterol, triglyceride, and FFA concentrations in TG and NTG mice after 3-months of high-fat feeding. ($n = 10$ in each group). Scale bars in **e**, 50 μm. Data are mean ± s.d. $^*P < 0.05$, $^{**}P < 0.01$, between the two genotypes indicated.

Metabolic analysis of energy balance using *Angptl6*$^{-/-}$ and *Angptl6* transgenic mice showed that one way AGF functions to regulate adiposity is through control of energy dissipation. Recent studies indicate that BAT and skeletal muscle regulate adaptive thermogenesis, which is mediated by PPARα, PPARδ, PPARγ and their coactivators, PGC-1α and PGC-1β, in response to energy overload[3,16,26,32–35]. We found statistically significant decreases in the expression of PPARα, PPARγ and PGC-1β in BAT and of PPARδ in skeletal muscle in *Angptl6*$^{-/-}$ mice, and increases in expression of PPARα, PPARγ and PGC-1β in BAT and of PPARα, PPARδ, and PGC-1α in skeletal muscle of *Angptl6* transgenic mice. In fact, *Angptl6* transgenic mice show phenotypes similar to those seen in transgenic mice with activated PPARδ[36–38] and PGC-1β[26]. Skeletal muscle is a direct target tissue of AGF, because AGF protein binds to C2C12 myocytes (**Supplementary Fig. 3** online). Treatment of C2C12 myocytes with AGF stimulated ligand activities of PPARα and PPARδ (**Supplementary Fig. 3**). Moreover, AGF activates p38 MAPK in muscle (**Supplementary Fig. 3**), which directly enhances the stabilization and activation of PGC-1 protein[34,35]. We therefore propose that AGF stimulates fat burning in peripheral tissues through the p38 MAPK pathway and downstream effects on respiration and gene expression linked to mitochondrial uncoupling and energy expenditure.

The microvasculature assists in heat dissipation at sites of active thermogenesis in peripheral tissues[28,29]. Because AGF increases the number of capillary-sized vessels in mice[8], we examined whether the vasculature is altered in *Angptl6*$^{-/-}$ and *Angptl6* transgenic mice. *Angptl6*$^{-/-}$ mice were susceptible to obesity and showed significantly ($P < 0.05$) decreased blood-flow perfusion in skeletal muscle, suggesting that loss of AGF enhances observed decreases in the efficiency in energy dissipation (**Supplementary Fig. 4** online). In parallel, a significant ($P < 0.01$) increase in the number of microvessels was observed in skeletal muscle of *Angptl6* transgenic mice, which may antagonize obesity by facilitat-

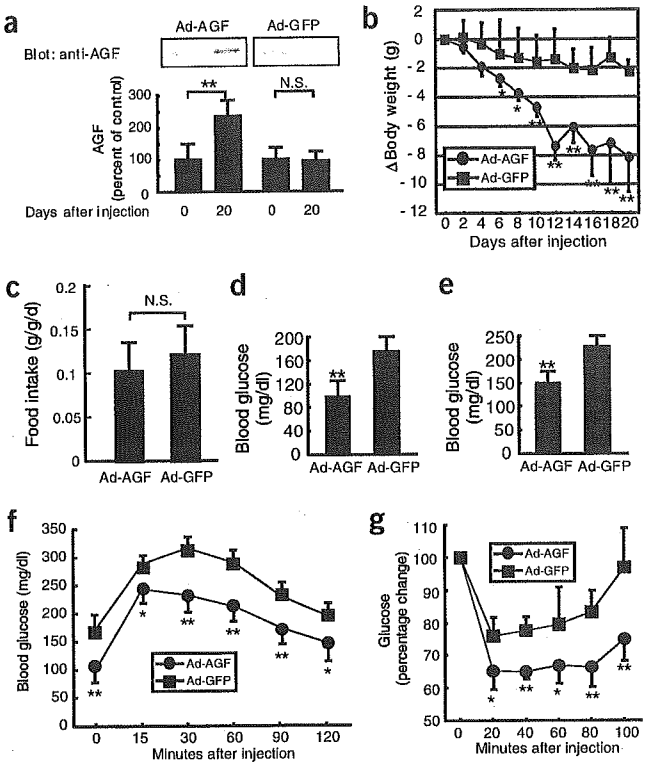

Figure 6 AGF decreased body weight and increased insulin sensitivity in high-fat fed-induced obese mice. (**a**) The relative ratio of serum concentrations of AGF in Ad-AGF injected and Ad-GFP injected mice on day 20 relative to each mouse on day 0. The value of serum AGF concentrations on day 0 is set at 100% ($n = 5$–8 in each group). (**b**) Alteration in body weight of high-fat fed-induced obese female mice after Ad-AGF and Ad-GFP injections ($n = 8$ in each group). (**c**–**g**) Comparison of food intake/lean body weight (**c**), fasting blood glucose (**d**), random fed blood glucose (**e**), glucose tolerance test (**f**) and insulin tolerance test (**g**) between Ad-AGF injected and Ad-GFP injected mice ($n = 5$–8 in each group). Data are mean ± s.d. $^*P < 0.05$, $^{**}P < 0.01$, between the two groups. N.S. indicates no significant difference compared with Ad-GFP–injected mice.

ing increases in energy dissipation. Furthermore, by providing a local angiogenic signal, AGF might increase the efficiency of lipid release from fat stores to maintain energy homeostasis. AGF induces angiogenesis in peripheral tissues, partially explaining how AGF counteracts obesity in addition to the direct effects of AGF on tissues functioning in adaptive thermogenesis.

Recent studies indicate that abnormal accumulation of triglycerides in muscle and liver results in insulin resistance by inhibiting insulin receptor signaling cascades[39,40]. Even on a high-fat diet, *Angptl6* transgenic mice are protected against hepatic and muscle steatosis, resulting in the maintenance of insulin sensitivity. These findings suggest that one mechanism whereby AGF affects insulin sensitivity is inhibition of abnormal lipid stores in insulin target tissues. Adipose tissue has a substantial impact on systemic glucose homeostasis through production of adipokines[34,35]. Recent studies show a role for adiponectin[20,21] and leptin[22,23] as mediators of insulin sensitivity and TNF-α[18,19] in mediating insulin resistance. In lipoatrophic diabetes, adiponectin and leptin deficiency resulting from lack of fat is associated with insulin resistance and diabetes[20,22,30,31]. Despite a greatly decreased WAT mass, *Angptl6* transgenic mice show increased insulin sensitivity, suggesting that AGF may increase insulin sensitivity. In contrast with decreased serum leptin levels, serum adiponectin levels in *Angptl6* transgenic mice were identical to those seen in wild-type mice. This may partially contribute to increased insulin sensitivity in *Angptl6* transgenic mice.

Findings derived from *Angptl6* transgenic mice, in which AGF expression is driven from the CAG promoter, led us to ask whether AGF in the circulation affects obesity and related metabolic abnormalities, because AGF is secreted primarily from hepatocytes. In this study, mice with high-fat diet–induced obesity overexpressing AGF in liver as a result of adenoviral transduction showed 2.5-fold increases in serum AGF levels over in controls and showed significant ($P < 0.01$) body weight loss and improved insulin sensitivity. Moreover, we observed that serum AGF levels in *Angptl6* transgenic mice described here and those seen in K14-*Angptl6* transgenic mice[7,8], in which AGF is driven by a skin-specific (K14) promoter, were approximately identical (**Supplementary Fig. 5** online). Notably, K14-*Angptl6* transgenic mice 8 months after birth show marked reduction in body weight and adiposity compared to controls, and this phenotype is similar to that seen in *Angptl6* transgenic mice created by driving *Angptl6* expression from the CAG promoter (**Supplementary Fig. 5**). K14-*Angptl6* transgenic mice also showed increased insulin sensitivity despite an extremely decreased WAT mass (**Supplementary Fig. 5**). These findings indicate that increasing serum AGF levels could counteract obesity and related insulin resistance, suggesting a physiological role of circulating AGF secreted from liver in antagonizing obesity.

Angptl3 is a circulating factor from liver functioning to regulate lipid metabolism[14,15]. Angptl4 is also predominantly expressed in liver and adipose tissue, and its expression is altered in nutrition and fasting, suggesting a role for Angptl4 in regulating fat metabolism[12,13]. Here, we show that AGF is a new hepatocyte-derived circulating factor counteracting high-fat-induced obesity and related insulin resistance through increased energy expenditure. Taken together with these findings, members of Angptl family function as endocrine factors with overlapping function secreted mainly from the liver to regulate metabolic homeostasis. As a next step to understand the role of Angptl family members in regulating metabolic homeostasis, identification of their cognate receptors and studies aimed at understanding their functional interactions are necessary.

In summary, we provide the first evidence that AGF directly antagonizes obesity and related insulin resistance. In addition to this direct effect, we propose that AGF-induced angiogenesis facilitates increased energy expenditure. Thus, AGF is a potential target for developing attractive pharmacological interventions counteracting obesity and related metabolic diseases.

METHODS

Gene targeting of *Angptl6*, generation of *Angptl6* transgenic mice, cell culture, transcription assays, western blot analyses and laser Doppler blood flow analysis. Please see **Supplementary Methods** online.

Blood analysis and tissue triglyceride assay. For IGTT, female mice were deprived of food 16 h and given 0.75 mg glucose per g body weight intraperitoneally; 3-month-old *Angptl6*$^{-/-}$ mice and controls and 4-month-old *Angptl6* transgenic mice and controls were used ($n = 5$–6 each). For IITT, female mice were given 0.75 U human insulin per kg body weight by subcutaneous injection; 3-month-old *Angptl6*$^{-/-}$ mice and controls and 4-month-old *Angptl6* transgenic mice and controls were used ($n = 5$–6 each). Blood was withdrawn from the supraorbital vein at indicated times. Blood glucose was measured by glucose oxidase method (Sanwa Kagaku). Serum FFA, triglyceride and cholesterol levels were determined by nonesterified fatty acid C-test, triglyceride L-type and cholesterol L-type (Wako), respectively. Plasma insulin was measured by insulin immunoassay (Eiken Kagaku).

Leptin, adiponectin and TNF-α were assayed by leptin assay kit (Linco Research Inc.), ELISA-based adiponectin immunoassay kit (Otsuka Seyaku) and ELISA-based TNF-α immunoassay kit (Techne Corporation), respectively, according to the manufacturer's instructions. Tissues were excised, weighed and homogenized. We added 500 μl of homogenates to 3 ml of methanol/chloroform at 1:2 (vol/vol). The mixture was shaken for 10 min and then centrifuged. We removed the organic layer and saved it, and re-extracted the aqueous layer with 3 ml of methanol/chloroform, and evaporated a small aliquot of the combined organic extracts. The triglyceride concentration of this aliquot was determined as described earlier.

Physiological measurements. For measurement of food consumption, 6-month-old *Angptl6*$^{-/-}$ mice and controls (n = 8 each), and 5-month-old *Angptl6*-transgenic mice and controls (n = 10 each) were housed individually. We measured consumption of food, as well as body weight, for 7 d consecutively. Mice were fed a normal chow diet (CE-2) or a high-fat diet (HFD-32) (CLEA). The high-fat diet study with 6-week-old *Angptl6* transgenic mice and controls was followed for a period of 12 weeks. Rectal temperature was monitored (6-month-old *Angptl6*$^{-/-}$ mice and controls (n = 8 each), and 5-month-old *Angptl6*-transgenic mice and nontransgenic control mice (n = 10 each)) using an electronic thermistor (Model BAT-12) equipped with a rectal probe (RET-3, Physitemp). Oxygen consumption (VO_2) was determined in 6-month-old *Angptl6*$^{-/-}$ mice and controls (n = 5 each), and 5-month-old *Angptl6*-transgenic mice and controls (n = 12 each), with an O_2/CO_2 metabolic measuring system (Model MK-5000, Muromachikikai) at 24 °C as described elsewhere[41]. Mice were kept unrestrained in the chamber for 24 h without food. We determined VO_2 when the minimum plateau shape was obtained during the light cycle, which corresponded to the period of sleep or inactivity. VO_2 is expressed as the volume of O_2 consumed per kilogram weight of lean body mass per minute.

Quantitative RT-PCR. Total RNA was isolated from the BAT and musculus gastrocnemius of mice (6-month-old *Angptl6*$^{-/-}$ mice and controls (n = 5 each), and 6-month-old *Angptl6*-transgenic mice and controls (n = 5 each)). Preparation of DNase-treated total RNA, reverse transcription, and PCR protocols were performed as previously described[8]. The oligonucleotides used for PCR are listed in **Supplementary Table 1** online. We monitored the levels of PCR products with an ABI PRISM 7700 sequence detection system and analyzed them with ABI PRISM 7700 SDS software (Applied Biosystems JAPAN Ltd). The relative abundance of transcripts was normalized to constitutive expression of 18sRNA, β-actin or HPRT mRNA.

CT scan analysis. The adiposity of mice was examined radiographically using CT (LaTheta, ALOKA) according to the manufacturer's protocol. We performed CT scanning at 2-mm intervals from the diaphragm to the bottom of the abdominal cavity.

Hepatic overexpression of AGF by adenoviral transduction. To prepare high-fat diet–induced obese mice, 8-week-old C57BL/6 female mice were fed a high-fat diet containing 32% (wt/wt) fat (HFD-32) for 12 months. Subsequently, mice with high-fat diet–induced obesity (n = 8) received 5×10^9 plaque-forming units (p.f.u.) of Ad-AGF. Serum AGF level was elevated by a single injection of Ad-AGF. For controls, mice with high-fat diet–induced obesity (n = 8) received 5×10^9 p.f.u. of Ad-GFP at the same time. We monitored body weight and food intake daily after intravenous injection of Ad-AGF and Ad-GFP. On day 16 after injection, random fed blood glucose levels were examined. Subsequently, IITT was performed. On day 20 after injection, we examined levels of serum AGF and fasting blood glucose. Subsequently, IGTT was performed.

Statistical analysis and ethical considerations. Results are expressed as the mean ± s.d. or mean ± s.e.m. Differences between groups were examined for statistical significance using Student t test or analysis of variance (ANOVA) with Fisher's PLSD test. The Ethics Review Committee for Animal Experimentation of Keio University approved the experimental protocol.

Note: Supplementary information is available on the Nature Medicine website.

ACKNOWLEDGMENTS

We thank K. Fukushima for her assistance with the experiments. This work was supported by Grants-in-Aid for Scientific Research on Priority Areas from the Ministry of Education, Science and Culture of Japan, by the Yamanouchi Foundation for Research on Metabolic Disorders and by the Mochida Memorial Foundation for Medical and Pharmaceutical Research.

COMPETING INTERESTS STATEMENT

The authors declare competing financial interests (see the *Nature Medicine* website for details).

Received 4 July 2004; accepted 25 January 2005
Published online at http://www.nature.com/naturemedicine/

1. Spiegelman, B.M. & Flier, J.S. Obesity and the regulation of energy balance. *Cell* **104**, 531–543 (2001).
2. Matsuzawa, Y., Funahashi, T. & Nakamura, T. Molecular mechanism of metabolic syndrome X: Contribution of adipokines adipocyte-derived bioactive substances. *Ann. NY Acad. Sci.* **832**, 146–154 (1999).
3. Lowell, B.B., & Spiegelman, B.M. Towards a molecular understanding of adaptive thermogenesis. *Nature* **404**, 652–660 (2000).
4. Levine, J.A., Eberhardt, N.L., & Jensen, M.D. Role of nonexercise activity thermogenesis in resistance to fat gain in human. *Science* **283**, 212–214 (1999).
5. Gale, N.W., & Yancopoulos, G.D. Growth factors acting via endothelial cell-specific receptor tyrosine kinases: VEGFs, Angiopoietins, and ephrins in vascular development. *Genes Dev.* **13**, 1055–1066 (1999).
6. Oike, Y. *et al.* Angiopoietin-related/like protein (ARPs/Angptls) regulate angiogenesis. *Int. J. Hematol* **80**, 21–28 (2004).
7. Oike, Y. *et al.* Angiopoietin-related growth factor (AGF) promotes epidermal proliferation, remodeling and regeneration. *Proc. Natl. Acad. Sci. USA.* **100**, 9494–9499 (2003).
8. Oike, Y. *et al.* Angiopoietin-related growth factor (AGF) promotes angiogenesis. *Blood* **103**, 3760–3766 (2004).
9. Kim, I. *et al.* Molecular cloning, expression, and characterization of angiopoietin-related protein. *J. Biol. Chem.* **274**, 26523–26528 (1999).
10. Camenisch, G. *et al.* ANGPTL3 stimulates endothelial cell adhesion and migration via Integrin αvβ3 and induces blood vessel formation *in vivo*. *J. Biol. Chem.* **277**, 17281–17290 (2002).
11. Ito, Y. *et al.* Inhibition of angiogenesis and vascular leakiness by Angiopoietin-related protein 4. *Cancer Res.* **63**, 6651–6657 (2003).
12. Yoon, J.C. *et al.* Peroxisome proliferator-activated receptor gamma target gene encoding a novel angiopoietin-related protein associated with adipose differentiation. *Mol. Cell Biol.* **20**, 5343–5349 (2000).
13. Kersten, S, *et al.* Characterization of the fasting-induced adipose factor FIAF, a novel peroxisome proliferator-activated receptor target gene. *J. Biol. Chem.* **275**, 28488–28493 (2000).
14. Koishi, R, *et al.* Angptl3 regulates lipid metabolism in mice. *Nat. Genet.* **30**, 151–157 (2002).
15. Inaba, T, *et al.* Angiopoietin-like protein 3 mediates hypertriglyceridemia induced by the liver X receptor. *J. Biol. Chem.* **278**, 21344–21351 (2003).
16. Evans, R.M., Barish, G.D. & Wang, Y.X. PPARs and the complex journey to obesity. *Nat. Med.* **10**, 355–361 (2004).
17. Spiegelman, B.M. & Flier, J.S. Adipogenesis and obesity: Rounding out the big picture. *Cell* **87**, 377–389 (1996).
18. Uysal, K.T., Wiesbrock, S.M., Marino, M.W. & Hotamisligil, G.S. Protection from obesity-induced insulin resistance in mice lacking TNF-α function. *Nature* **389**, 610–614 (1997).
19. Peraldi, P., Xu, M. & Spiegelman, B.M. Thiazolidinediones block tumor necrosis factor-a-induced inhibitor of insulin signaling. *J. Clin. Invest.* **100**, 1863–1869 (1997).
20. Yamauchi, T. *et al.* The fat-derived hormone adiponectin reverses insulin resistance associated with both lipoatrophy and obesity. *Nat. Med.* **7**, 941–946 (2001).
21. Berg, A.H., Combs, T.P., Du, X., Brownlee, M. & Scherer, P.E. The adipocyte-secreted protein Acrp30 enhances hepatic insulin action. *Nat. Med.* **7**, 647–653 (2001).
22. Shimomura, I., Hammer, R.E., Ikemoto, S., Brown, M.S. & Goldstein, J.L. Leptin reverses insulin resistance and diabetes mellitus in mice with congenital lipodystrophy. *Nature* **401**, 73–76 (1999).
23. Friedman, J.M. Obesity in the new millennium. *Nature* **404**, 632–634 (2000).
24. Lowell, B.B., *et al.* Development of obesity in transgenic mice after genetic ablation of brown adipose tissue. *Nature* **366**, 740–742 (1993).
25. Zurlo, F., Larson, K., Bogardus, C. & Ravussin, E. Skeletal muscle metabolism is a major determinant of resting energy expenditure. *J. Clin. Invest.* **86**, 1423–1427 (1990).
26. Kamei, Y. *et al.* PPARγ coactivator 1β/ERR ligand 1 is an ERR protein ligand, whose expression induces a high-energy expenditure and antagonizes obesity. *Proc. Natl. Acad. Sci. USA.* **100**, 12378–12383 (2003).
27. Niwa, H., Yamamura, K. & Miyazaki J. Efficient selection for high-expression transfectants with a novel eukaryotic vector. *Gene* **108**, 193–200 (1991).
28. Sierra-Honigmann, M.R. et al. Biological action of leptin as an angiogenic factor. *Science* **281**, 1683–1686 (1998).
29. Sarmiento, U., *et al.* Morphologic and molecular changes induced by recombinant human leptin in the white and brown adipose tissues of C57BL/6 mice. *Lab. Invest.* **77**, 243–256 (1997).
30. Shimomura, I. *et al.* Insulin resistance and diabetes mellitus in transgenic mice expressing nuclear SREBP-1c in adipose tissue: model for congenital generalized lipodystrophy. *Genes Dev.* **12**, 3182–3194 (1998).
31. Gavrilova, O. *et al.* Surgical implantation of adipose tissue reverses diabetes in

lipoatrophic mice. *J. Clin. Invest.* **105**, 271–278 (2000).
32. Moller, D.E. & Berger, J.P. Role of PPARs in the regulation of obesity-related insulin sensitivity and inflammation. *Int. J. Obes. Relat. Metab. Disord.* **27**, S17–S21 (2003).
33. Wu, Z., *et al.* Mechanisms controlling mitochondrial biogenesis and respiration through the thermogenic coactivator PGC-1. *Cell* **98**, 115–124 (1999).
34. Puigverger, P. *et al.* Cytokine stimulation of energy expenditure through p38 MAP kinase activation of PPARγ coactivator-1. *Mol. Cell* **8**, 971–982 (2001).
35. Puigserver, P. & Spiegelman, B.M. Peroxisome proliferator-activated receptor-γ coactivator 1α (PGC-1α): Transcriptional coactivator and metabolic regulator. *Endocr. Rev.* **24**, 78–90 (2003).
36. Wang, Y.X. *et al.* Peroxisome-proliferator-activated receptor δ activates fat metabolism to prevent obesity. *Cell* **113**, 159–70 (2003).
37. Tanaka, T. *et al.* Activation of peroxisome proliferator-activated receptor delta induces fatty acid beta-oxidation in skeletal muscle and attenuates metabolic syndrome. *Proc. Natl. Acad. Sci. USA.* **100**, 15924–15929 (2003).
38. Dressel, U. *et al.* The peroxisome proliferatior-activated receptor β/δ agonist, GW501516, regulates the expression of genes involved in lipid catabolism and energy uncoupling in skeletal muscle cells. *Mol. Endocrinol.* **17**, 2477–2493 (2003).
39. Shulman, G.I., *et al.* Cellular mechanisms of insulin resistance. *J. Clin. Invest.* **106**, 171–176 (2000).
40. Petersen, K.F. *et al.* Mitochondrial dysfunction in the elderly: Possible role in insulin resistance. *Science* **300**, 1140–1142 (2003).
41. Barger, P.M., Browning, A.C., Garner, A.N. & Kelly, D.P. p38 mitogen-activated protein kinase activates peroxisome proliferator-activated receptor α: a potential role in the cardiac metabolic stress response. *J. Biol. Chem.* **276**, 44495–44501 (2001).

Available online at www.sciencedirect.com
SCIENCE DIRECT®
Journal of Molecular and Cellular Cardiology 40 (2006) 24–34
Journal of Molecular and Cellular Cardiology
www.elsevier.com/locate/yjmcc

Original article

A strategy of retrograde injection of bone marrow mononuclear cells into the myocardium for the treatment of ischemic heart disease

Shin-Ichiro Yokoyama [a], Noboru Fukuda [a,b,*], Yuxin Li [a], Kazuhiro Hagikura [a], Tadateru Takayama [a], Satoshi Kunimoto [a], Junko Honye [a], Satoshi Saito [a], Mika Wada [b], Aya Satomi [b], Maiko Kato [b], Hideo Mugishima [b], Yoshiaki Kusumi [c], Masako Mitsumata [c], Toyoaki Murohara [d]

[a] *Department of Medicine, Nihon University School of Medicine, 30-1, Ooyaguchi-kamimachi, Itabas..., Tokyo 173-8610, Japan*
[b] *Department of Advanced Medicine, Division of Cell Regeneration and Transplantation, Nihon University School of Medicine, Tokyo 173-8610, Japan*
[c] *Department of Pathology, Nihon University School of Medicine, Tokyo 173-8610, Japan*
[d] *Department of Cardiology, Nagoya University Graduate School of Medicine, Nagoya 466-8550, Japan*

Received 10 February 2005; received in revised form 25 May 2005; accepted 16 June 2005

Available online 04 November 2005

Abstract

Objective. – Bone marrow cells implantation (BMI) has been reported to efficiently improve ischemic heart disease. However, BMI strategies are generally invasive. To establish a BMI strategy for ischemic heart disease, we performed implantation of autologous cryopreserved mononuclear cells (MNCs) from bone marrow (BM) retrogradely into the myocardium via the coronary vein in pigs with acute myocardial infarction (AMI) and old myocardial infarction (OMI).

Methods. – BM cells were harvested from the pigs' fumurs. MNCs were collected by centrifugation and were cryopreserved. Anterior myocardial infarction was induced by occlusion of the midportion of the left anterior descending coronary artery without surgical intervention. Frozen BM cells were quickly thawed and injected retrogradely via the coronary vein into the myocardium through a single balloon infusion catheter 6 h and 2 weeks after the induction of infarction. Four weeks after implantation, coronary arteriograms were obtained, cardiac function was analyzed with the use of a conductance catheter, and histopathologic anlysis was performed with a confocal laser microscope. Plasma levels of natriuretic peptides and angiogenic growth factors were measured after BMI.

Results. – Flow cytometric analysis revealed that 90% of cryopreserved BM cells were viable in vitro. Labeled BM cells were entirely distributed around in the infarcted area of maycardium in pigs. BMI increased collateral neovasculralization *in infarcted hearts*. BMI significantly improved cardiac function in *AMI with BMI and OMI with BMI groups*. BMI also increased the formation of microcapillary arteries in infarcted hearts. Levels of natriuretic peptides were significantly decreased, and levels of vascular endothelial growth factor (VEGF) and *basic* fibroblast growth factor (*FGF2*) were significantly increased after BMI. Confocal laser microscopy revealed the presence of proliferative and activated myocardial cells in infarcted hearts after BMI.

Conclusion. – The retrograde infusion of cryopreserved BM cells into myocardium efficiently induced angiogenesis and improved cardiac function in pigs with AMI or OMI. These results suggest that the present strategy of BMI will be safe and feasible as an angiogenic cell therapy for ischemic heart disease.

Keywords: Ischemic heart disease; Regenerative medicine; Bone marrow cell; Angiogenesis; Retrograde infusion; Cryopreservation

1. Introduction

Current standard treatments for acute myocardial infarction (AMI) are predominantly based on reperfusion of the obstructive coronary arteries by thrombolysis with tissue plasminogen activator (tPA) and/or by percutaneous coronary intervention (PCI). Therapeutic approaches to the management of myocardial ischemia including *angina* pectoris and old myocardial infarction (OMI) commonly include manipulations designed to reduce myocardial oxygen demand or to

* Corresponding author. Tel.: +81 3 3972 8111; fax: +81 3 3972 8666.
E-mail address: fukudan@med.nihon-u.ac.jp (N. Fukuda).

0022-2828/$ - see front matter © 2005 Elsevier Ltd. All rights reserved.
doi:10.1016/j.yjmcc.2005.06.008

increase blood supply to ischemic area mechanically by coronary artery bypass grafting (CABG) or PCI with medication. The recovery of cardiac function after infarction is important, because the mortality of patients with AMI remains high. Alternative therapies include those of *induction* the development of new collateral vessels.

Transfer of angiogenic genes such as those of vascular endothelial growth factor (VEGF) and *basic fibroblast growth factor* (*FGF2*) has been reported to increase collateral blood flow and to improve cardiac function in cases of chronic myocardial ischemia [1,2]. The gene therapies raise a number of practical issues for application in human trials, including the development of adequate delivery systems and safety [3,4].

Autologous cell therapy for induction of angiogenesis is thought to be more progressive regenerative treatment. Bone marrow (BM) includes abundant stem cells [5] and endothelial progenitor cells [6,7]. Therapeutic Angiogenesis using Cell Transplantation (TACT) Study Investigators reported that BM cell implantation (BMI) improves ischemic ulcers in cases of limb ischemia by improving blood flow [8]. Thus, BMI has been considered for application in ischemic heart disease [9,10].

Direct injection into the myocardium and *intra-coronary* infusion are methods of delivery of BM cells to the ischemic heart [11,12]. In addition, catheter-based injection of cells into the ischemic area has recently been reported [13,14]. Because these procedures are invasive, require special techniques and are costly, they cannot be performed in general hospitals. In addition, in occluded coronary arteries with poor collaterals, transplanted cells may not reach the target ischemic lesion. Less invasive angiogenic cell transplantation into the ischemic heart are therefore necessary. Regenerative cell therapies for ischemic heart disease have not been established.

The harvest of BM cells can be dangerous for patients with severe ischemic heart disease because it can cause anemia or hypovolemia. Thus, preservation of BM cells from patients and the ability of preserved BM cells to induce agniogenesis should be evaluated.

To establish an efficient strategy of BMI for ischemic heart disease, we cryopreserved BM cells and delivered the cells retrogradely via the coronary vein to the myocardium in pigs. We evaluated the ability of this method to induce angiogenesis and its effect on cardiac function in pigs with AMI and OMI.

2. Materials and methods

This study conformed to the *Guide for the Care and Use of Laboratory Animals* published by the US National Institutes of Health (NIH Publication No. 85-23, revised 1996).

2.1. Preparation and cryopreservation of BM mononuclear cells (BM-MNCs)

All surgical procedures were performed under general anesthesia and continuous electrocardiographic (ECG) and blood pressure monitoring. Adult male pigs (35 kg) were premedicated with ketamine (20 mg/kg, im) before induction of anesthesia with 4% isoflurane. Anesthesia was maintained with 1–2.5% isoflurane. A volume of 400 ml of peripheral blood was obtained 2 weeks before BM harvest and we created a transfusion bag of red cell concentrate in mannnitol-adenine-phosphate solution (RC-MAP, Terumo Medical Co.) from those blood. A half volume of RC-MAP was used for autologous blood transfusion to improve anemia at the harvest and the rest was used in combination with BM blood at the isolation of MNCs to be full-filled the collected bag. All pigs received an infusion of iron (Tontetsu, Pfizer Pharmacy, 50 mg/day) for 3. Those with a red blood cell count $>3.5 \times 10^6$ per ml were included in the experiments. Two weeks later, 400 ml of BM cells were harvested bilaterally from the femurs of all pigs. During harvest, the pigs were received 200 ml of autologous blood transfusion for 1 h. After harvest, MNCs were collected by the use of program modifications (MNC software Version 5.1, BMP) of the COBE Spectra Apheresis System (Gambro BCT, Inc.). Five milliliters of dimethyl sulfoxide and 10% dextran 40 (Terumo) were added to 20 ml of the collected MNCs-enriched blood [15]. For implantation of preserved BM cells, the collected MNCs were cryopreserved with an auto-preserved liquid nitrogen system (CryoMed, Futaba Medical) according to the following protocol: pre-freeze rate 10 °C/min, start freeze temperature at –3 °C, end freeze temperature at –10 °C to –15 °C, post-freeze rate 2 °C/min and end temperature at –50 °C.

2.2. Flow cytometric analysis and colony forming unit

The thawed BM-MNCs were stained with a green fluorescent marker PKH2-GL (Sigma Chemical Co.). The PKH-GL is the green fluorescent cell linker kit for general cell membrane labeling. At first, we determined the optimal dye/cell concentration. After the centrifuging collected cells ($400 \times g$) for 5 min, we carefully aspirated the supernatant on the pellet and labeled the half of implanted cells using PKH2-GL labeling kit. After the labeling, the cells were analyzed by flow cytometry (FACS Calibur, Becton Dickinson). The parts of the thawed BM-MNCs ($N = 11$) were analyzed by flow cytometry before the implantation with the use of 7-amino-actinomycin D (7AAD) (VIA-PROBE™, Becton Dickinson) to evaluate the cell viability.

Preserved cell content was evaluated by plating 50,000 cells in 1.1% methylcellulose (Stem Cell Technologies) supplemented with 30% fetal bovine serum (FBS) and 50 ng/ml interleukin (IL)-3, or with 30% FBS and a cytokine mixture (2 ng/ml IL-3, 25 ng/ml stem cell factor, 5 ng/ml granulocyte-macrophage colony stimulating factor and 2 U/ml human erythropoietin). We determine the timing colony forming units from the following manual (Colony Assays of Hematopietic Cells Using Methylcellulose Media; Terry Fox Laboratory Media Preperation Service) [16]. Fourteen days culture is enough time to make the colony for leukocyte-progenitor cells. Seven days is only enough time to assess CFU-E. Colo-

nies (>50 cells) were counted after 14 days in culture at 37 °C, 5% CO_2. Colonies were classified as colony forming unit-granulocyte/monocyte (CFU-GM), burst-forming unit-erythroid (BFU-E) from an early erythroid progenitor or CFU-Mix, a more immature, multipotent type of colony that containing cells from myeloid and erythroid lineages.

2.3. Induction of myocardial infarction

We performed right and left coronary arteriography (CAG) after injection of 2.5 mg of isosorbide-dinitrate (ISDN) into each coronary artery under general anesthesia. The *pigs* were subjected to acute antero-septal myocardial infarction by implantation of beads of 2.0 mm in diameter with 0.8 mm holes into the mid portion of the left anterior descending coronary artery (LAD) through a *guide-wire*. After placement, coronary occlusion occurred gradually with increasing thrombi around the beads. Occlusion of the LAD was confirmed angiographically after 6 h. All procedures were performed *under* fluoroscopic guidance.

2.4. Animal groups and BMI

Twenty-one pigs were randomly assigned to one of four groups, AMI without BMI (AMI control, $N = 5$), AMI with BMI ($N = 6$), OMI without BMI (OMI control, $N = 5$) or OMI with BMI ($N = 5$). BM-MNCs were *cryopreserved* for 2 and 4 weeks for the AMI and OMI groups, respectively (Fig. 1). Frozen MNCs were quickly thawed at 37 °C, washed with 5% serum albumin and 10% dextran 40 and then centrifuged at 400 × *g* at 10 °C for 10 min.

To deliver BM-MNCs retrogradely via the coronary vein to the myocardium, we advanced a single balloon catheter (Nipro Inc.) through the coronary sinus into the anterior intraventricular vein (AIV) and positioned it near the occlusive site of the LAD. Coronary veins run parallelly most of the coronary arteries on the surface of the heart. From these anatomical features, it is very easy to access the target lesions. MNCs from BM were stained with PKH2-GL and continuously infused at 10 ml/h for 4 h from 6 h after induction of myocardial infarction.

To evaluate the distribution of cells, four pigs were injected cells retrogradely and their hearts were removed 3 and 6 h after the injection. The distribution rate was evaluated by counting fluorescent cells in each area. The ratio of fluorescent cells was calculated as following: number of positive cells existed in the anterior (target) area/number of positive cells existed in the non-anterior (non-target) area × 100%. Three horizontal sections (5 mm proximal site, occlusive site and 5 mm distal site) were selected.

Thawed MNCs were infused continuously through the coronary vein catheter into the LAD area, including the ischemic border and infarct areas for 4 h under of ECG observation. Hemodynamics analysis was performed 6 h and 2 weeks after infarction for the AMI with BMI and the OMI with BMI groups, respectively. The same volumes of saline were infused through the catheter in each control group.

2.5. Evaluation of cardiac function and blood data

A 7F thermodilution catheter (Baxter Healthcare Corp.) was placed in the pulmonary artery via percutaneous femoral approach to evaluate hemodynamic status. Several cardiac parameters were evaluated by a conductance method (Millar Instrument Inc.). The LV pressure–volume study was performed before and 4 weeks after the intervention in all animals. A 10-electrode conductance catheter and a micromanometer-tipped catheter (Millar Instrument Inc.) were inserted into the left ventricle and connected to a signal-conditioner processor (Leycom Sigma-5; CardioDynamics BV) for pressure and volume recording. Pressure–volume relations were obtained at steady state with atrial pacing (100 bpm).

We introduced 4F size heparinized endhole-type catheter (ANTHRON P-U catheter, TORAY) through the cervical vein into the coronary sinus in every pigs. To collect blood samples after intervention, we connected the P-U catheter and P-U Celesite Port (PT-5L, TORAY). We collected the samples at

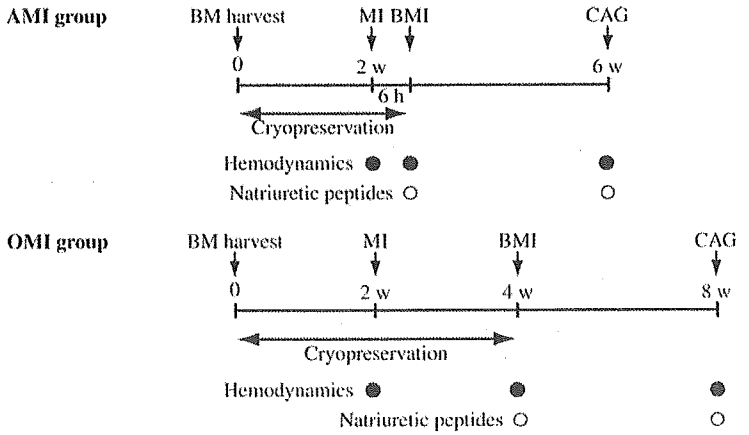

Fig. 1. Experimental design for the induction myocardial infarcts, BM cell implantation, evaluation of hemodynamics, measurement of natriuretic peptides and angiogenic growth factors and angiography in pigs. BM = bone marrow, MI = induction of myocardial infarction, CAG = coronary angiography, w = weeks.

3, 7, 14, 28 days after the intervention. Plasma levels of VEGF and FGF2 were measured with an ELISA kit (R&D Systems). Plasma levels of atrial natriuretic peptide (ANP) and brain natriuretic peptide (BNP) were measured with a radioimmunoassay kit (Yamasa Shoyu) from peripheral blood. Blood chemistry data were evaluated in the same blood samples.

2.6. Angiography and evaluation of coronary flow reserve

Selective CAG was performed to detect collateral sources. Collateral indices were assigned as follows: 0 = no visible collaterals, 1 = collateral formation visible only with contrast stain, 2 = partial filling of the main epicardial vessel, 3 = complete filling of the distal LAD.

We also measured coronary flow reserve as the function of vessels. Coronary flow velocities were measured with a Doppler Flowire (Cardiometrics, Inc., Mountain View, USA). The Flowire™ is a 175 cm long, flexible, steerable angioplasty guide wire, 0.014 in. in diameter, with a 12 MHz piezoelectric ultrasound transducer at its tip. The velocity data are processed on-line by fast Fourier transformation and displayed with a real-time gray scale spectral display. The Flowire was then advanced into LAD and was positioned just proximal site of the occluded lesion to obtain a stable blood flow velocity signal. Baseline flow velocities under ISDN drip were obtained and arterial pressure and heart rate were recorded. The following intra-coronary Doppler parameters were measured: diastolic to systolic velocity ratio (DSVR), average peak velocity (APV) during the procedure. Coronary flow reserve (CFR) was calculated the ratio max APV and baseline APV.

2.7. Histopathology

All pigs were killed with overdoses of intravenous injections of pentobarbital and potassium chloride, and their hearts were removed after CAG. PKH2-GL labeled tissues obtained from the ischemic region were snap-frozen. Each heart was fixed in 20% formaldehyde, and 5-μm-thick sections, including the whole area at risk were obtained (Leica RM2145 microtome, Leica Instruments) and treated with hematoxylin and eosin (HE) and Masson trichrome stain.

To confirm the proliferative activity of cells, we stained selected specimens from control and treated groups simultaneously with anti-MIB-1 antibody. MIB-1 (Ki67) antigen is expressed throughout the cell cycle and is a reliably distinguishes proliferation. Fluorescence detection of the labeled proliferative cells through staining with fluorochromated avidin [avidin-Alexa Fluor 488™ (green fluorescence), DAKO Japan Corp., dilution 1:500]. Tissues were also stained for α-sarcomeric actin as a marker of myocardial cells. Simultaneous immunofluorescence detection of myocardial markers using the appropriate primary antibodies and secondary antibodies conjugated to the fluorochromes [Alexa Fluor 633™ (infrared fluorescence), DAKO, dilution 1:500]. Fluorescent signals were detected by optical sectioning using a Leica TCS-NT confocal laser-scanning microscope (Leica Instruments). Vessel walls were stained for α-smooth muscle actin (α-SMA) (Becton Dickinson), antibody to evaluate vascular development. Because of the lack of appropriate markers for pig endothelium, we evaluated myocardial microvessel density (microvessels per mm^2), microvessel mean area measured from α-SMA immunostained sections atzb 200 magnifications from five fields of each section. Hansen-Smith et al. [17] reported the increase in the number of microvessels only partially covered by α-SMA suggests arteriolization of capillaries.

To quantify coronary artery, the vessel number and the total vessel area including the adventitial layer of the epicardial coronary artery, was measured in sections 5 mm *distal* the occlusive site. Myocardial microvessel area (cm^2) in sections of 5 mm *distal* the occlusive site were also measured in α-SMA immunostained sections [18].

We determined the fibrosis content of the myocardium with an automatic image analysis system, by planimetric analysis (NIH Image 1.61/ppc). We evaluated the entire area of each histologic section 10 mm *distal* the occlusive site. Masson Trichrome stain sections were used for detection the fibrotic area. The infarct area was calculated according to fibrosis grade (fibrosis area/total area × 100%).

2.8. Statistical analysis

All results are presented as mean ± S.D. The significance of differences between mean values was evaluated by Student's *t*-test for unpaired data and by two-way analysis of variance (ANOVA) followed by Duncan's multiple range tests. P values < 0.05 were considered statistically significant.

3. Results

3.1. Characteristics of isolated BM cells

FACS analysis of BM cells stained with PKH2-GL showed that the separated cells included many type of cells including MNCs, lymphocytes, granulocytes and red blood cells, the population of MNCs was the largest (86 ± 8.8% of BM cells) (data not shown).

The number of MNCs in 400 ml of femoral BM used for implantation into the myocardium was $3.2 \pm 1.2 \times 10^9$ ($N = 11$) after separation. Recovery of viable BM cells from cryopreservation was 87.5 ± 6.9% ($N = 11$). This reagent (7AAD) is used as a viability probe for methods of dead cell exclusion. Thus 7AAD was used for evaluation of cell viability. Myeloid and erythroid cells were assessed by colony assay before and after cryopreservation of separated MNCs and prior to implantation. The recovery of colony forming progenitor cells after cryopreservation of separated MNCs is shown in Table 1. Colony forming progenitor cells catego-

Table 1
Recovery of colony forming progenitor cells after cryopreservation of the separation of MNCs

	CFU-GM	BFU-E	CFU-Mix	Total
Fresh MNCs	38 ± 6	10 ± 4	26 ± 3	76 ± 10
Cryopreserved MNCs	35 ± 6	9 ± 2	28 ± 5	72 ± 9

Colony forming unit (CFU); fresh (prior to preservation) and preserved cell content was evaluated by plating 50,000 cells in 1.1% methylcellulose supplemented with 30% FBS and 50 ng/ml IL-3, or with 30% FBS and a cytokine mixture (2 ng/ml IL-3, 25 ng/ml SCF, 5 ng/ml GM-CSF and 2 U/ml human erythropoietin). Colonies (>50 cells) were counted after 14 days in culture at 37 °C, 5% CO_2. Colonies were classified into the groups following CFU-granulocyte/monocyte (CFU-GM), burst-forming unit-erythroid (BFU-E) from an early erythroid progenitor or CFU-Mix. Data are the mean ± S.D. There are no significant differences between fresh and cryopreserved MNCs.

rized as CFU-GM, BFU-E or CFU-Mix were completely recovered after cryopreservation, indicating that cryopreservation after separation caused no significant loss of the enriched progenitor cells from the myeloid or erythroid lineages which are vital for transplant engraftment.

3.2. Distribution of BM-MNCs via coronary vein catheter

The distribution of BM-MNCs stained with PKH2-GL and injected retrogradely via the coronary vein into the infarcted heart is shown in Fig. 2. Over 90% of labeled MNCs were found around in the infarcted area, and the remaining cells were found only in the left circumflex coronary artery (LCX) area 3 h after injection. Labeled MNCs were not identified in the injured myocardium after *intra-coronary* infusion in hearts from pigs with AMI (data not shown). Fig. 2A shows a cineangiogram of contras medium injection to AIV. The injected medium distributed apex lesion in pig heart. It is clearly visible green color indicates fluorescence of cells in infracted heart (Fig. 2C–E). Injected MNCs were attached to vessel walls (Fig. 2C) and were present in the myocardium (Fig. 2D, E) 6 h after the injection.

3.3. Angiogenesis after BMI

Collateral vessels were observed in all groups. However, antegrade flow due to bridge collaterals was observed only in the BMI groups (Fig. 3A). Collateral index of the BMI groups were significantly higher than that in the control groups (Fig. 3B). However, the collateral flow findings existed only around areas of infarction. These collateral vessels were too small size to be visible in cineangiograms. Thus, the retrograde administration of BM-MNCs via the coronary vein resulted in a directional increase in collateral circulation that was regionally restricted to the left coronary system.

Data from a Doppler Flowire show BMI therapy increased coronary flow reserve both in AMI and OMI (but not significantly). Increasing coronary flow reserve equal to increasing bet of functional micro vessels (data not shown).

3.4. Cardiac function after BMI

Changes in cardiac function before and 6 h or 2 weeks after induction of the myocardial infarction in the AMI and OMI groups with or without BMI are shown in Fig. 4. End-diastolic volume (EDV) was significantly lower in AMI and OMI groups than the control groups 4 weeks after BMI. Ejection fraction (EF) was significantly higher in the AMI and OMI groups than the control groups 4 weeks after BMI. End-diastolic pressure (EDP) was significantly lower in the AMI group but not in the OMI group than in the control groups at 4 weeks after BMI.

3.5. Levels of natriuretic peptides and angiogenic growth factors after BMI

ANP levels in peripheral blood were significantly increased in the AMI control but not in the OMI groups. ANP levels 4 weeks after BMI were significantly lower in the AMI group than in the control group. BNP levels in peripheral blood were significantly increased in the OMI groups but not in the AMI

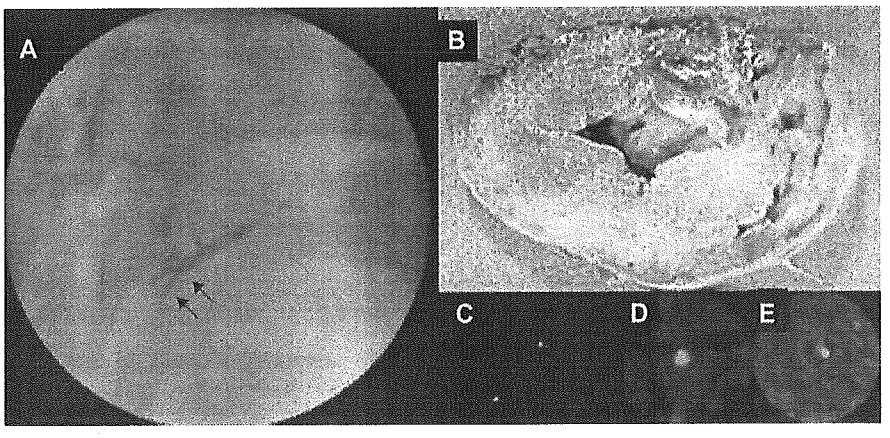

Fig. 2. Distribution of bone marrow mononuclear cells (BM-MNCs) injected retrogradely into infarcted heart. Cells were stained with a green fluorescent marker, PKH2-GL, and injected via the coronary vein 6 h after induction of myocardial infarction. (A) A cineangiogram of contras medium injection to AIV. The injected medium distributed apex lesion of pig heart. (B) Distribution of fluorescent cells in all areas of the section 3 h after injection. Presence of fluorescent cells (C) in vessel walls and (D, E) in the myocardium 6 h after injection.

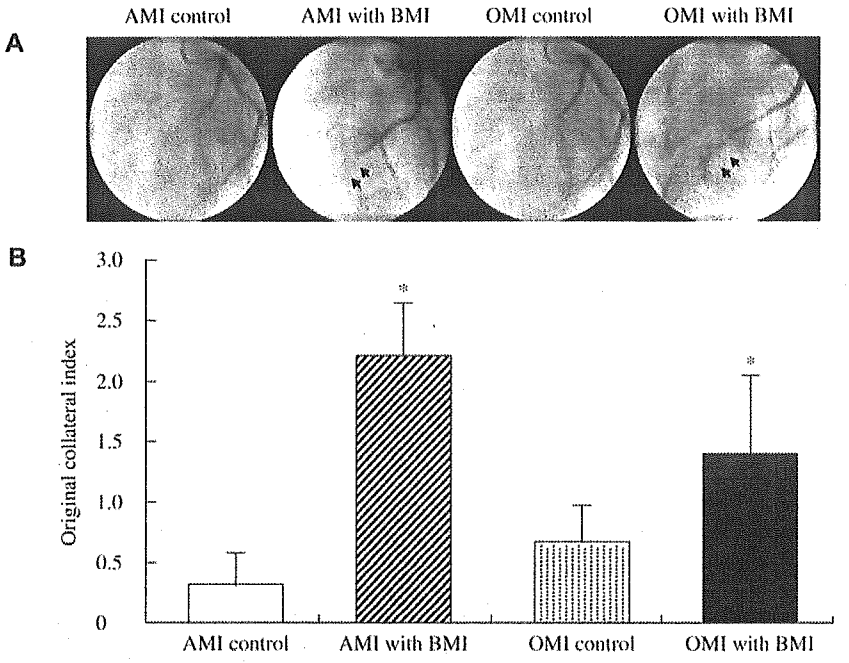

Fig. 3. Coronary angiography in pigs with acute or old myocardial infarcts with BM cell implantation (AMI with BMI or OMI with BMI). (A) Selective coronary angiographies were recorded from an RAO 30 view. Arrows indicate antegrade flow due to bridge collaterals. (B) Collateral indices. Collateral index were rated according to the following: 0 = no visible collaterals, 1 = collateral formation only with contrast stain, 2 = partial filling of the main epicardial vessel, 3 = complete filling of the distal LAD. Data are the mean ± S.D. ($N = 5$). *$P < 0.05$ vs. each control.

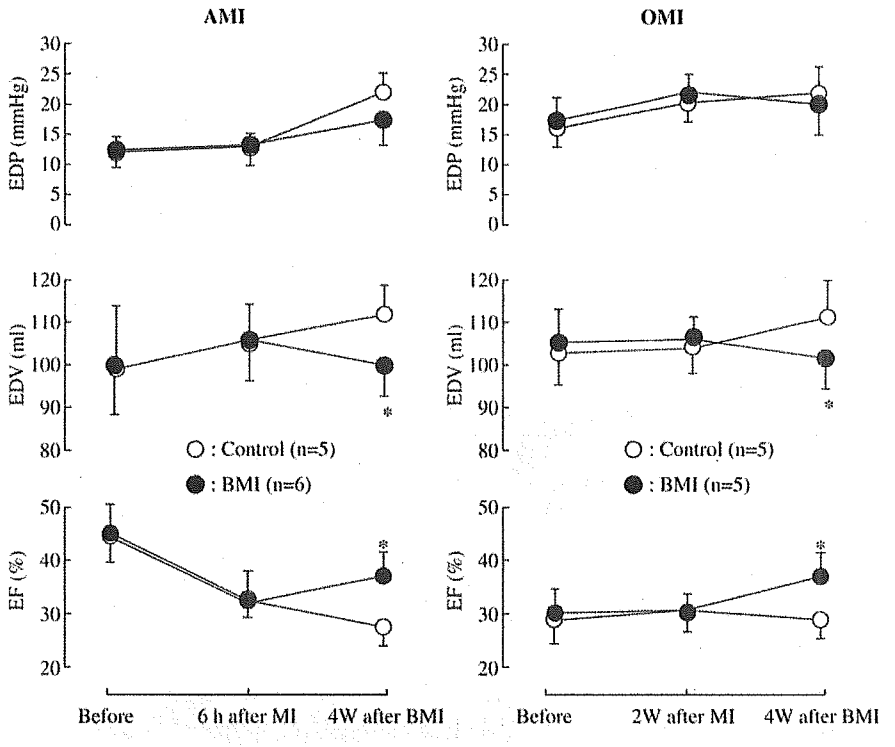

Fig. 4. Changes in cardiac function after BMI before and 6 h or 2 weeks after induction of myocardial infarction (MI) in the AMI group or the OMI group, and 4 weeks after BMI in each group. Several LV parameters, EDP, EDV, and EF were evaluated with the conductance method. Data are the mean ± S.D. *$P < 0.05$ vs. each control.

groups. BNP levels 4 weeks after BMI were significantly lower in the AMI and OMI groups with BMI than that in the control groups (Table 2).

Levels of *FGF2* and VEGF were significantly increased in the AMI and OMI groups 3 days after BMI in comparison to levels in the control groups (data not shown).

Table 2
Levels in natriuretic peptides in peripheral blood after BMI

		6 h	4 weeks
ANP	AMI control	89 ± 26	154 ± 48 [b]
(pg/ml)	AMI with BMI	105 ± 38	72 ± 25 [a]
BNP	AMI control	232 ± 56	200 ± 56
(pg/ml)	AMI with BMI	225 ± 49	129 ± 34 [a]
		2 weeks	6 weeks
ANP	OMI control	181 ± 31	189 ± 29
(pg/ml)	OMI with BMI	175 ± 28	174 ± 17
BNP	OMI control	39 ± 6	151 ± 15 [b]
(pg/ml)	OMI with BMI	42 ± 5	105 ± 18 [a,b]

Plasma levels of ANP and BNP in peripheral blood in pigs 6 h and 4 weeks after induction of myocardial infarction in the AMI group and OMI group and 4 weeks after BMI in each group were measured by radioimmunoassay. Data are the mean ± S.D.

[a] $P < 0.05$ vs. each control.

[b] $P < 0.05$ vs. 6 h in the AMI group and 2 weeks in the OMI group.

3.6. Histopathologic findings after BMI

Four weeks after BMI in the AMI group, PKH2-GL fluorescence was observed by confocal laser scopy in mature vessels walls (Fig. 5A) and in the microvascular system in the preserved myocardium around the infarcted area (Fig. 5B).

We counted the number of α-SMA positive microvessels in the infarcted areas 5 mm *distal to* the occlusive site. The number of microvessels *as capillary artery* under 100 μm in diameter was significantly higher in infarcted hearts from the AMI with BMI and OMI with BMI groups than in hearts from the control groups. There were no significant differences in the number of microvessels with multilayer smooth muscle over 100 μm in diameter between the BMI groups and the control groups (Fig. 6A). α-SMA-positive cells were predominantly identified in the epicardium. In particular, there were more microvascular areas in the epicardium close to the occlusive site of the LAD in the BMI groups (Fig. 6B). Some sections from implanted hearts showed growing cardiac muscle fibers around vessels (Fig. 7A). By confocal laser microscopy, MIB-1-positive cells (green) and α-sarcomeric actin-positive cells (red) were observed around microvessels and were located around the infarct area implanted with BM-MNCs, and double-positive cells (yellow) were observed only in hearts from the AMI with BMI group (Fig. 7B1–B3). In the OMI with BMI it was rare for us to detect the double-positive cells. The number of double-positive cells was much less or none in the control groups than BMI group (Fig. 7B4–B6).

With respect to the effect of BMI on cardiac fibrosis, fibrosis contents were smaller, but not significantly, in hearts from the BMI groups than those from control groups (AMI control vs. AMI with BMI = 23.5 ± 8.4% vs. 17.5 ± 5.1%, OMI control vs. OMI with BMI = 24.6 ± 9.5% vs. 19.8 ± 7.8%).

4. Discussion

To establish an efficient BMI strategy for ischemic heart disease, we implanted cryopreserved BM-MNCs via the coronary vein into the myocardium of pigs with AMI or OMI. We observed good recovery of viable cells from cryopreservation and improved cardiac function with antegrade collateral neovasculalization and increased numbers of microvessels in pigs with AMI as well as those with OMI.

BMI is reported to increase regional blood flow and improve cardiac function in pigs with myocardial infarction [19,20]. However, BM cells were injected into the heart by open-chest surgery in these studies. Cell delivery into the myocardium can occur via the *intra-coronary artery or intra-coronary* vein and by direct injection under open-chest or closed-chest surgery. Catheter-based cell delivery is an easier and less invasive method. Assmus et al. [11] recently reported that autologous BM-MNCs via balloon catheter, which placed into the coronary artery, repair the infarcted myocardium in

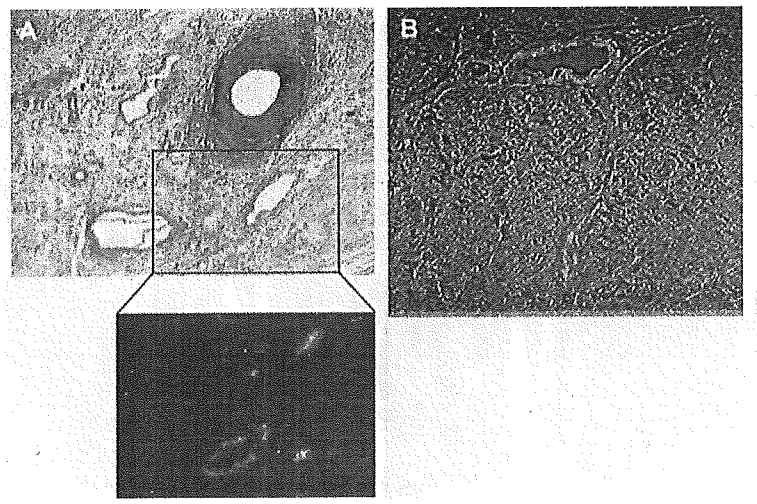

Fig. 5. Histologic findings of ischemic areas in hearts from pigs with AMI 4 weeks after BMI. PKH2-GL-labeled tissues obtained from the ischemic region were snap-frozen. (A) Angiography during cell infusion. (B) Preserved myocardium around infarcted area stained with hematoxylin and eosin (original magnification × 100). Lower panel indicates green fluorescence observed in mature vessels walls. (C–E) Confocal laser microscopic findings (original magnification C × 40. D, E × 400).

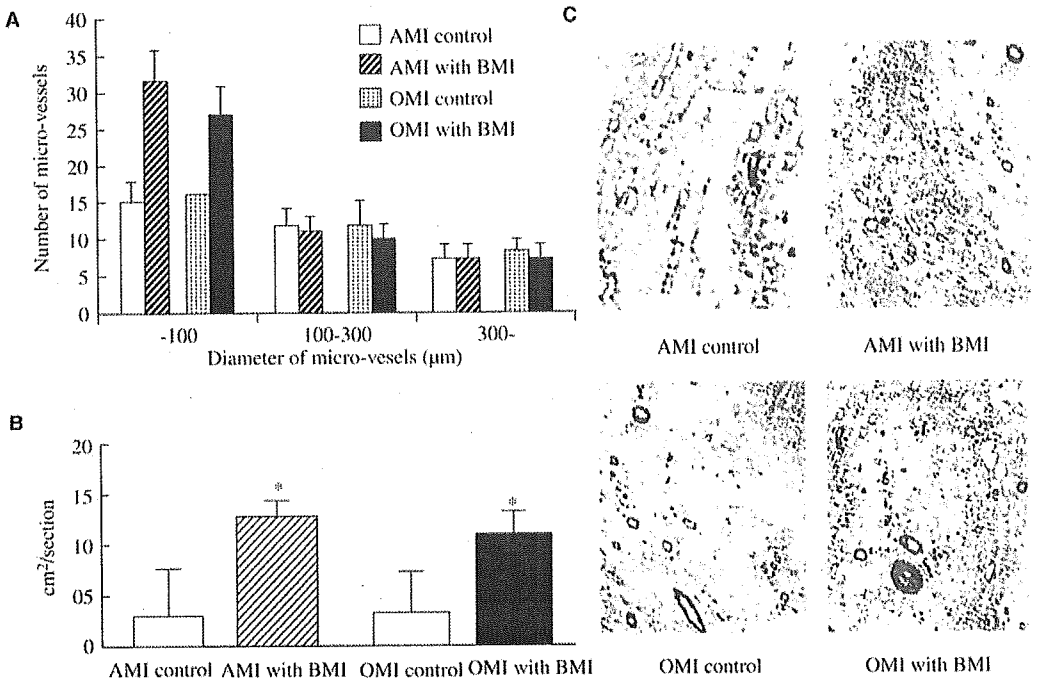

Fig. 6. Number and density of microvessels in the infarcted areas of heart from pigs with AMI or OMI 4 weeks after BMI. (A) Number of α-smooth muscle actin-positive microvessels in sections 5 mm above the occlusive site. Microvessel diameters were classified as 100, 100–300 and over 300 μm. (B) Myocardial microvessel area (cm^2) in sections 10 mm under the occlusive site. Data are the mean ± S.D. $^*P < 0.05$ vs. each control. (C) Representatives of α-SMA positive microvessels in infracted heart from pigs of each group (original magnification × 400).

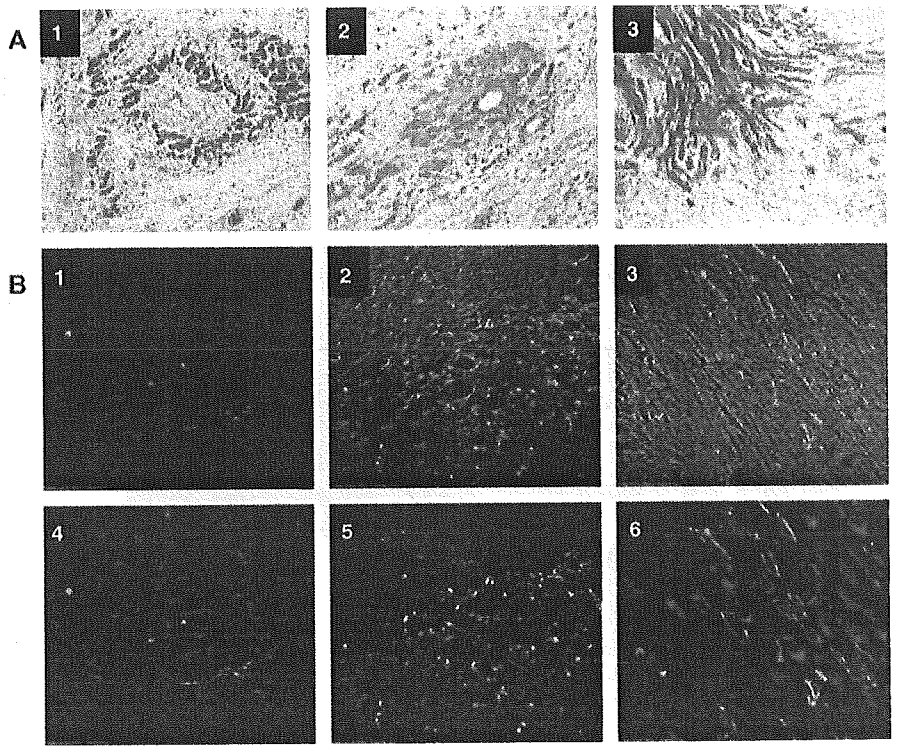

Fig. 7. (A) Cardiac muscle around vessels in the infarcted areas 4 weeks after BMI (original magnification × 400, Masson trichrome stain). (A1) AMI control. (A2) AMI with BMI. (A3) OMI with BMI. Confocal laser microscopy of MIB-1-positive cells (green), α-sarcomeric actin-positive cells (red) around micro-vessels and located around the infarct area implanted with BMMNCs, and double-positive cells (yellow) (B1, 4). AMI control, (B2, 5) AMI with BMI, (B3, 6) OMI with BMI.

patients with AMI. However, BM cells administered via *intra-coronary* infusion attached poorly to the myocardium because of the high value of blood flow in the coronary artery.

Kawamoto et al. [21] recently emphasizes the importance of sorted endothelial progenitor cells for transplantation in ischemic diseases. Endothelial progenitor cells are source for angiogenic cell therapy. On the other hand, whole bone marrow implantation (BMI), not sorted cells, has been established as a clinical therapy for hematopoetic diseases including leukemia. CD34-riched BM cells is an important key for this therapy. Furthermore cryopreservation is one of the sorting methods. Rubinstein et al. [15] reported almost all hematopoietic colony forming cells present in placental/umbilical cord blood units can be recovered in a uniform volume of 20 ml by using rouleaux formation induced by hydroxyethyl starch and centrifugation to reduce the bulk of erythrocytes and plasma and, thus, concentrate leukocytes. But they used cryopreserved whole MNCs from placental/umbilical cord blood, so we needed to confirm the viability and CFU of pig BM. From these considerations the cryopreserved BM cells are powerful source for clinical application.

Recently, Thompson et al. [22] reported efficient delivery of BM cells to the normal heart in pigs via the coronary vein. We were also able to efficiently and safely deliver BM-MNCs to the injured myocardium in pigs with myocardial infarction via the coronary vein. The retrograde infusion of BM cells via coronary vein is easy same as *intra-coronary* artery BMI or direct injection under open-chest surgery. In addition, this *retrograde infusion* method can be performed in any *hospital with cineangiogram systems* by interventional cardiologists. The retrograde infusion of BM cells is considered to be more effective than intra-coronary infusion because the venous system is fully open, whereas the coronary artery is obstructed in any patients with coronary diseases.

Catheter-based direct implantation of BM cells with the use of *an* electrical mapping system has been reported [14,19]. However, this system requires expensive special equipment and operators for the mapping technique. Retrograde infusion via the coronary vein is advantageous with respect to cost and time performance. Catheter-based trans-coronary vein infusion has been used successfully to deliver solutions of reporter genes such as VEGF and *FGF2* [18,22,23]. In the present study, collateral flow was observed 7 days after BMI and indicated that retrograde infusion does not compromise the function of injected cells.

BM-MNCs include abundantly progenitor or stem cells, that can differentiate to a variable of cell type. BM stromal cells, also called mesenchymal stem cells, can differentiate into mature cells of multiple mesenchymal tissues including adipose, bone and cartilage [5]. In the present study, the fluorescence labeled BM-MNCs differentiated into endothelial cells around the infarcted area, suggesting that BM-MNCs do not differentiate into a variable of cells in arterial systems in vivo.

The substantial increases in myocardial perfusion obtained in the present study were accompanied by histologic evidence of increased numbers of microcapillaries under 100 μm in diameter. These histologic results should be supported by CAG findings with positive contrast media stain. However, the fluoroscope could not be used to evaluate coronary microvascular beds because of its limited spatial resolution of 200 μm. There are reported discrepancies between coronary flow and histologic findings [24,25]. Functional coronary capillaries are well known to comprise coronary flow reserve, which has been defined as the ratio of coronary resistance under control (rest) conditions to coronary resistance after maximal coronary vasodilation [26]. In the present study, a Doppler Flowire study show BMI therapy more increased coronary flow reserve both in AMI and OMI compare to each control groups (but not significantly). The increased numbers of microcapillaries are in fact directly associated with increases in myocardial perfusion flow to improve LV function. However, microcapillaries, which are not assessed by conventional angiography, are suboptimal as extracardiac collaterals.

In the present study, the retrograde infusion of cryopreserved BM cells into the myocardium efficiently induced angiogenesis characterized by the formation of α-SMA-positive microvessels with diameters under 100 μm. BMI did not increase the number of vessels with diameters over 100 μm. Abundant numbers of α-SMA-positive cells in vessels under 100 μm in diameter were predominantly located near an epicardial artery around the infarcted area than in fibrotic areas near the apex. MIB-1- and α-sarcomeric actin-double-positive cells were observed at area in hearts implanted with BM cells. Moreover, MIB-1-positive cells were also found in vessel tubular structures in the implanted area. These findings suggest the presence of proliferative and activated myocardial cells induced by BMI and that the myocardial cells were protected from cell death caused by acute ischemia.

Angiogenesis is a process of microvascular network formation that involves several mechanisms, including sprouting, growth and remodeling of the initial network [27]. The recruitment of smooth muscle cells and pericytes around endothelial cells stabilizes the primitive vascular tube and is also essential for maturation of the developing vessel. The angiogenic process is tightly regulated by sequential expression of several angiogenic growth factors, chemokines, adhesion molecules and proteolytic enzymes. The increased shear stress induces the development of collateral vessels through the expression of angiogenic growth factors such as *FGF2*, which is produced by activated monocytes [27]. Furthermore, high-grade coronary stenosis provokes myocardial ischemia, and ischemic cardiomyocytes produce and release VEGF, which is a key for angiogenic factors [28]. In the present study, levels of *FGF2* and VEGF in coronary veins were increased only in the AMI and OMI groups after BMI. Increases in plasma levels VEGF and *FGF2* have also reported in patients with AMI [29,30]. In addition, Hamano et al. [31] reported that increases in expression of VEGF and *FGF2* in autologous implanted BM cells in hypoxic tissue, indicated that implanted BM cells produce angiogenic growth factors

under hypoxic conditions to enhance angiogenesis in the ischemic heart. Since blood samples for cytokine measurement were selectively collected from coronary vein not from peripheral blood, they directly reflect myocardial cytokines. Because *increased* levels of VEGF and *FGF2* were identified only in our BMI groups, these angiogenic cytokines are likely related to the process of α-SMA-positive microvascular network formation and proliferation.

In the present study, we confirmed that cryopreserved BM-MNCs are viable and that they considerably improve cardiac function in pigs with AMI or OMI. These findings indicated that cryopreserved stem cells or progenitor cells could be made available as regenerative treatment for ischemic heart disease. Patients with prior myocardial infarction are more than three times as likely to have infarcts as those without prior myocardial infarction [32]. It is possible that infusion of preservation of BM cells from those patients will *be* an effective treatment for *subsequent myocardial infarction.*

Refractory angina and ischemic cardiomyopathy are multivessel diseases that are resistant to treatment with CABG, PCI and medicines and are suitable target diseases for BMI. We induced AMI in pigs as a model AMI and OMI and of ischemic heart conditions such as human ischemic cardiomyopathy and refractory angina pectoris. However, since all of pigs had no coronary diseases before creation of myocardial infarction, establishment of such animal models in pigs is practically difficult. It has been reported the ischemic and injured hearts produce abundant angiogenic cytokines, and that the conditions of injured tissues produce potential factors to repair these tissues [33–35]. In the present study, only non-necrotic myocardium was preserved, and the amount of myogenesis was less than the amount of angiogenesis. The pathologic examination showed that the volume of the ischemic myocardium determined the recovery of LV function. The amount of preserved and recovered myocardium after BMI was greater in hearts with AMI than in hearts with OMI. Thus the baseline condition of the patient determines the amount of recovery after cell therapy. We believe that the most suitable target ischemic heart disease for BMI is AMI. It is very difficult to recover from poor cardiac function accompanied by decreased LV volume, these hearts require additional regenerative therapy.

In conclusion, retrograde infusion of cryopreserved BM cells into the myocardium efficiently induced angiogenesis and improved cardiac function in pigs with AMI or OMI, suggesting that the present BMI strategy will be a clinically safe and feasible angiogenic cell therapy for ischemic heart disease.

Acknowledgements

This work was supported in part by a Grant-in Aid for the High-Tech Research Center from the Japanese Ministry of Education, Science, Sports, and Culture to Nihon University and by a grant from New Energy and Industrial Technology Development Organization (NEDO).

References

[1] Symes JF, Losordo DW, Vale PR, Lathi KG, Esakof DD, Mayskiy M, et al. Gene therapy with vascular endothelial growth factor for inoperable coronary artery disease. Ann Thorac Surg 1999;68:830–6.

[2] Grines CL, Watkins MW, Helmer G, Penny W, Brinker J, Marmur JD, et al. Angiogenic gene therapy (AGENT) trial in patients with stable angina pectoris. Circulation 2002;105:1291–7.

[3] Losordo DW, Vale PR, Hendel RC, Milliken CE, Fortuin FD, Cummings N, et al. Phase 1/2 placebo-controlled, double-blind, dose-escalating trial of myocardial vascular endothelial growth factor 2 gene transfer by catheter delivery in patients with chronic myocardial ischemia. Circulation 2002;105:2012–8.

[4] Vale PR, Losordo DW, Milliken CE, McDonald MC, Gravelin LM, Curry CM, et al. Randomized, single-blind, placebo-controlled pilot study of catheter-based myocardial gene transfer for therapeutic angiogenesis using left ventricular electromechanical mapping in patients with chronic myocardial ischemia. Circulation 2001;103: 2138–43.

[5] Herzog EL, Chai L, Krause DS. Plasticity of marrow-derived stem cells. Blood 2003;102:3483–93.

[6] Asahara T, Murohara T, Sullivan A, Silver M, van der Zee R, Li T, et al. Isolation of putative progenitor endothelial cells for angiogenesis. Science 1997;275:964–7.

[7] Asahara T, Masuda H, Takahashi T, Kalka C, Pastore C, Silver M, et al. Bone marrow origin of endothelial progenitor cells responsible for postnatal vasculogenesis in physiological and pathological neovascularization. Circ Res 1999;85:221–8.

[8] Tateishi-Yuyama E, Matsubara H, Murohara T, Ikeda U, Shintani S, Masaki H, et al. Therapeutic Angiogenesis using Cell Transplantation (TACT) Study Investigators. Therapeutic angiogenesis for patients with limb ischaemia by autologous transplantation of bone-marrow cells: a pilot study and a randomised controlled trial. Lancet 2002; 360:427–35.

[9] Orlic D, Kajstura J, Chimenti S, Bodine DM, Leri A, Anversa P. Transplanted adult bone marrow cells repair myocardial infarcts in mice. Ann N Y Acad Sci 2001;938:221–9.

[10] Orlic D, Kajstura J, Chimenti S, Jakoniuk I, Anderson SM, Li B, et al. Bone marrow cells regenerate infarcted myocardium. Nature 2001; 410(6829):701–5.

[11] Assmus B, Schachinger V, Teupe C, Britten M, Lehmann R, Dobert N, et al. Transplantation of progenitor cells and regeneration enhancement in acute myocardial infarction (TOPCARE-AMI). Circulation 2002;106:3009–17.

[12] Strauer BE, Brehm M, Zeus T, Kostering M, Hernandez A, Sorg RV, et al. Repair of infarcted myocardium by autologous intracoronary mononuclear bone marrow cell transplantation in humans. Circulation 2002;106:1913–8.

[13] Tse HF, Kwong YL, Chan JK, Lo G, Ho CL, Lau CP. Angiogenesis in ischaemic myocardium by intramyocardial autologous bone marrow mononuclear cell implantation. Lancet 2003;361:47–9.

[14] Fuchs S, Satler LF, Kornowski, Okubagzi P, Weisz G, Baffour R, et al. Catheter-based autologous bone marrow myocardial injection in no-option patients with advanced coronary artery disease: a feasibility study. J Am Coll Cardiol 2003;41:1721–4.

[15] Rubinstein P, Dobrila L, Rosenfield RE, Adamson JW, Migliaccio G, Migliaccio AR, et al. Processing and cryopreservation of placental/umbilical cord blood for unrelated bone marrow reconstitution. Proc Natl Acad Sci USA 1995;92:10119–22.

[16] Eaves CJ, Eaves AC. Fundamental control of hematopoiesis. In: Fissher J, editor. Biochemical pharmacology of blood and bloodforming organs, handbook of experimental pharmacology, (vol. 101). Berlin: Springer Verlag; 1992. p. 5–31.

[17] Hansen-Smith F, Egginton S, Hudlicka O. Growth of arterioles in chronically stimulated adult rat skeletal muscle. Microcirculation 1998;5:49–59.

[18] Rutanen J, Rissanen TT, Markkanen JE, Gruchala M, Silvennoinen P, Kivela A, et al. Adenoviral catheter-mediated intramyocardial gene transfer using the mature form of vascular endothelial growth factor-D induces transmural angiogenesis in porcine heart. Circulation 2004; 109:1029–35.

[19] Kamihata H, Matsubara H, Nishiue T, Fujiyama S, Tsutsumi Y, Ozono R, et al. Implantation of bone marrow mononuclear cells into ischemic myocardium enhances collateral perfusion and regional function via side supply of angioblasts, angiogenic ligands, and cytokines. Circulation 2001;104:1046–52.

[20] Tomita S, Mickle DA, Weisel RD, Jia ZQ, Tumiati LC, Allidina Y, et al. Improved heart function with myogenesis and angiogenesis after autologous porcine bone marrow stromal cell transplantation. J Thorac Cardiovasc Surg 2002;123:1132–40.

[21] Kawamoto A, Tkebuchava T, Yamaguchi J, Nishimura H, Yoon YS, Milliken C, et al. Intramyocardial transplantation of autologous endothelial progenitor cells for therapeutic neovascularization of myocardial ischemia. Circulation 2003;107:461–8.

[22] Thompson CA, Nasseri BA, Makower J, Houser S, McGarry M, Lamson T, et al. Percutaneous transvenous cellular cardiomyoplasty. A novel nonsurgical approach for myocardial cell transplantation. J Am Coll Cardiol 2003;41:1964–71.

[23] von Degenfeld G, Raake P, Kupatt C, Lebherz C, Hinkel R, Gildehaus FJ, et al. Selective pressure-regulated retroinfusion of fibroblast growth factor-2 into the coronary vein enhances regional myocardial blood flow and function in pigs with chronic myocardial ischemia. J Am Coll Cardiol 2003;42:1120–8.

[24] Lund GK, Watzinger N, Saeed M, Reddy GP, Yang M, Araoz PA, et al. Chronic heart failure: global left ventricular perfusion and coronary flow reserve with velocity-encoded cine MR imaging: initial results. Radiology 2003;227:209–15.

[25] Thornburg KL, Reller MD. Coronary flow regulation in the fetal sheep. Am J Physiol 1999;277:R1249–R1260.

[26] Strauer BE. The concept of coronary flow reserve. J Cardiovasc Pharmacol 1992;19(Suppl 5):S67–80.

[27] Yancopoulos GD, Davis S, Gale NW, Rudge JS, Wiegand SJ, Holash J. Vascular-specific growth factors and blood vessel formation. Nature 2000;407:242–8.

[28] Simons M, Bonow RO, Chronos NA, Cohen DJ, Giordano FJ, Hammond HK, et al. Clinical trials in coronary angiogenesis: issues, problems, consensus: an expert panel summary. Circulation 2000; 102:E73–E86.

[29] Fujita M, Ikemoto M, Kishishita M, Otani H, Nohara R, Tanaka T, et al. Elevated basic fibroblast growth factor in pericardial fluid of patients with unstable angina. Circulation 1996;94:610–3.

[30] Tamura K, Nakajima H, Rakue H, Sasame A, Naito Y, Nagai Y, et al. Elevated circulating levels of basic fibroblast growth factor and vascular endothelial growth factor in patients with acute myocardial infarction. Jpn Circ J 1999;63:357–61.

[31] Hamano K, Li TS, Kobayashi T, Kobayashi S, Matsuzaki M, Esato K. Angiogenesis induced by the implantation of self-bone marrow cells: a new material for therapeutic angiogenesis. Cell Transplant 2000;9: 439–43.

[32] Haffner SM, Lehto S, Ronnemaa T, Pyorala K, Laakso M. Mortality from coronary heart disease in subjects with type 2 diabetes and in nondiabetic subjects with and without prior myocardial infarction. N Engl J Med 1998;339:229–34.

[33] Waltenberger J. Modulation of growth factor action: implications for the treatment of cardiovascular diseases. Circulation 1997;96:4083–94.

[34] Post MJ, Laham R, Sellke FW, Simons M. Therapeutic angiogenesis in cardiology using protein formulations. Cardiovasc Res 2001;49: 522–31.

[35] Gustafsson T, Bodin K, Sylven C, Gordon A, Tyni-Lenne R, Jansson E. Increased expression of VEGF following exercise training in patients with heart failure. Eur J Clin Invest 2001;31:362–6.

Available online at www.sciencedirect.com
SCIENCE DIRECT®
Biochemical and Biophysical Research Communications 341 (2006) 973–978
BBRC
www.elsevier.com/locate/ybbrc

Fenofibrate activates AMPK and increases eNOS phosphorylation in HUVEC ☆

Hisashi Murakami [a], Ryuichiro Murakami [a,*], Fukushi Kambe [b], Xia Cao [b], Ryotaro Takahashi [a], Toru Asai [a], Toshihisa Hirai [a], Yasushi Numaguchi [a], Kenji Okumura [a], Hisao Seo [b], Toyoaki Murohara [a]

[a] *Department of Cardiology, Nagoya University Graduate School of Medicine, 65 Tsurumai, Showa-ku, Nagoya 466-8550, Japan*
[b] *Department of Endocrinology and Metabolism, Division of Molecular and Cellular Adaptation, Research Institute of Environmental Medicine, Nagoya University, Furo-cho, Chikusa-ku, Nagoya 464-8601, Japan*

Received 6 January 2006
Available online 24 January 2006

Abstract

Fenofibrate improves endothelial function by lipid-lowering and anti-inflammatory effects. Additionally, fenofibrate has been demonstrated to upregulate endothelial nitric oxide synthase (eNOS). AMP-activated protein kinase (AMPK) has been reported to phosphorylate eNOS at Ser-1177 and stimulate vascular endothelium-derived nitric oxide (NO) production. We report here that fenofibrate activates AMPK and increases eNOS phosphorylation and NO production in human umbilical vein endothelial cells (HUVEC). Incubation of HUVEC with fenofibrate increased the phosphorylation of AMPK and acetyl-CoA carboxylase. Fenofibrate simultaneously increased eNOS phosphorylation and NO production. Inhibitors of protein kinase A and phosphatidylinositol 3-kinase failed to suppress the fenofibrate-induced eNOS phosphorylation. Neither bezafibrate nor WY-14643 activated AMPK in HUVEC. Furthermore, fenofibrate activated AMPK without requiring any transcriptional activities. These results indicate that fenofibrate stimulates eNOS phosphorylation and NO production through AMPK activation, which is suggested to be a novel characteristic of this agonist and unrelated to its effects on peroxisome proliferator-activated receptor α.

Keywords: Fenofibrate; AMP-activated protein kinase; Endothelial nitric oxide synthase; Nitric oxide; Human umbilical vein endothelial cells

Fenofibrate, one of the peroxisome proliferator-activated receptor α (PPARα) agonists, has been in use for the treatment of dyslipidemia, mainly due to its ability to lower triglyceride levels, raise high-density lipoprotein levels, and decrease the levels of small, dense low-density lipoprotein particles [1]. A clinical study in patients with type 2 diabetes has reported that fenofibrate reduces the progression of atherosclerotic lesions [2]. In addition, fenofibrate has been demonstrated to improve endothelial function as estimated by flow-mediated dilatation [3,4]. These beneficial effects of fenofibrate may be partly due to an improvement of the lipid profile and a direct anti-inflammatory action on endothelial cells, which express PPARα [5,6]. On the other hand, a recent study has reported that fenofibrate upregulates eNOS activity in vascular endothelial cells, suggesting that this direct effect, leading to nitric oxide (NO) production, may contribute to the improvement of endothelial function [7].

Endothelium-derived NO is an important mediator of cardiovascular protection [8], and the ability of endothelial cells to synthesize this short-lived molecule is widely used as a marker of normal function. The generation of NO by endothelial nitric oxide synthase (eNOS) is governed by multiple molecular mechanisms, which include the regulation of eNOS expression and phosphorylation and the

☆ *Abbreviations:* AMPK, 5′-AMP-activated protein kinase; eNOS, endothelial nitric oxide synthase; HUVEC, human umbilical vein endothelial cells.

* Corresponding author. Fax: +81 52 744 2177.
E-mail address: ryuichi@med.nagoya-u.ac.jp (R. Murakami).

0006-291X/$ - see front matter © 2006 Elsevier Inc. All rights reserved.
doi:10.1016/j.bbrc.2006.01.052

participations of many cofactors [9]. It has recently been reported that the phosphorylation at Ser-1177 of eNOS, which plays an important role in the regulation of eNOS activity, is induced by AMP-activated protein kinase (AMPK) [10], and AMPK-induced phosphorylation results in NO production in endothelial cells [11]. AMPK is a sensor that maintains intracellular energy homeostasis and mediates a number of physiological signals, such as inhibition of cholesterol, fatty acid, and protein synthesis, and enhancement of glucose uptake and blood flow [12–14]. For example, adiponectin stimulates NO production through AMPK-induced eNOS phosphorylation in endothelial cells [15]. Although fenofibrate has been reported to increase eNOS expression, leading to upregulation of eNOS [7], whether fenofibrate increases eNOS phosphorylation has not been clarified. In addition, the effects of fenofibrate on AMPK, which is one of the molecules that mediate the signal of endothelial NO production in vascular endothelial cells, have not been elucidated. Together, these findings prompted us to explore the connection between fenofibrate and the AMPK pathway or eNOS phosphorylation. The aims of the present study were to investigate whether fenofibrate activates AMPK and increases eNOS phosphorylation and NO production in vitro. We show here that fenofibrate activates AMPK and increases eNOS phosphorylation without requiring PPARα activity in endothelial cells.

Materials and methods

Materials. Cell culture media and supplements were purchased from Kurabo Industries (Osaka, Japan). Fenofibrate was a kind gift from Kaken Pharmaceutical (Tokyo, Japan). Fetal bovine serum (FBS) was purchased from Gibco, Invitrogen (Carlsbad, CA). Wortmannin was purchased from EMD Biosciences (La Jolla, CA). Anti-phosphorylated AMPKα (Thr-172), AMPKα, phosphorylated acetyl-CoA carboxylase (ACC) (Ser-79), phosphorylated eNOS (Ser-1177), phosphorylated Akt (Thr-308), and Akt antibodies were from Cell Signaling Technology (Beverly, MA). Anti-eNOS antibody was from BD Biosciences (San Jose, CA). Detergent compatible protein assay reagents were purchased from Bio-Rad Laboratories (Hercules, CA). Immobilon-P polyvinylidene fluoride membrane was from Millipore (Bedford, MA). Can Get Signal Immunoreaction Enhancer Solutions were purchased from Toyobo (Osaka, Japan). The ECL Western blotting detection kit was purchased from Amersham Biosciences (Buckinghamshire, UK). Diaminofluorescein-2 diacetate (DAF-2/DA) was purchased from Daiichi Pure Chemicals (Tokyo, Japan). All other reagents were purchased from Sigma (St. Louis, MO). Wortmannin, H-89, actinomycin D, cycloheximide, bezafibrate, WY14643, and fenofibrate were dissolved in dimethyl sulfoxide (DMSO). In every experiment performed, the final DMSO concentration was equal among all groups and less than 0.2%.

Cell culture. HUVEC were isolated essentially as described by Jaffe et al. [16] and cultured in an endothelial growth medium, HuMedia-EG2, supplemented with 2% FBS, 10 ng/mL human epithelial growth factor, 5 ng/mL human fibroblast growth factor-B, 1 μg/mL hydrocortisone, 10 μg/mL heparin, 50 μg/mL gentamicin, and 50 ng/mL amphotericin B. The culture medium was exchanged every 48 h. HUVEC up to passage six were used for the experiments. Nearly confluent HUVEC were then cultured for 6 h in FBS-free medium supplemented with 0.2% bovine serum albumin (BSA).

SDS–polyacrylamide gel electrophoresis and Western blotting. The serum-starved monolayers were lysed in heated Laemmli buffer, boiled for 10 min, sonicated, and centrifuged. After protein quantification, the resulting supernatant was fractionated by 7.5–10% SDS–polyacrylamide gel electrophoresis and transferred onto Immobilon-P. Membranes were blocked with 5% BSA and incubated with primary antibodies. The Can Get Signal Immunoreaction Enhancer Solutions 1 and 2 were used for dilution of primary and peroxidase-labeled secondary antibodies, respectively. Immunocomplexes were detected using the ECL Western blotting detection kit and quantified by densitometry. For assessment of the amount of each protein expressed, the membranes were left at 50 °C for 30 min in 62.5 mM Tris/HCl buffer (pH 6.8) containing 100 mM 2-mercaptoethanol and 2% SDS followed by three washes, blocking, and an additional three washes. The membranes were then re-blotted with primary antibodies.

Spectrofluorimetric determination of NO released from endothelial cells. NO levels were estimated using DAF-2/DA fluorescent dye as described by Nakatsubo et al. [17]. HUVEC were grown to confluence on a 24-well microplate. After treating the cells with FBS-free medium for 2 h, the culture medium was exchanged with phosphate-buffered saline supplemented with 0.5 mM $MgSO_4$, 0.9 mM $CaCl_2$, 0.2% BSA, and 100 μM L-arginine, followed by 15 min incubation with or without 500 μM N_ω-nitro-L-arginine methyl ester (L-NAME). After 10 min incubation with 1 μM DAF-2/DA and 20 μM fenofibrate, the fluorescence was measured with a Fluoroskan Ascent CF fluorescence plate reader (MTX Lab Systems, Vienna, VA) with excitation at 485 nm and emission at 527 nm at 37 °C. For quantification, MAHAM NONOate was used as a standard NO donor. The fluorescence of the wells without cells was measured and subtracted in order to correct the DAF-2/DA auto-fluorescence under each condition.

Statistical analysis. Statistical differences between continuous variables and treatment groups were determined by one-way analysis of variance (ANOVA) followed by Scheffe's post hoc test. Two-way ANOVA with repeated measures over time followed by Scheffe's post hoc test was used to compare the changes in chemiluminescence intensity from baseline at each time among the treatment groups. Values of $p < 0.05$ were considered significant.

Results

Fenofibrate increased eNOS phosphorylation and NO production in HUVEC

First, we investigated the effects of fenofibrate on eNOS phosphorylation and expression in HUVEC. Fenofibrate treatment induced a rapid and significant increase in eNOS phosphorylation at Ser-1177. This increase was observed from 2.5 to 10 min after treatment (Figs. 1A and B). Although fenofibrate is known to increase eNOS expression, the total eNOS protein level was not altered over the 10 min.

We next examined the phosphorylation of AMPK and Akt, which are upstream kinases for eNOS [9]. In the same manner as eNOS, fenofibrate markedly increased phosphorylation of AMPK at Thr-172, whereas it did not increase phosphorylation of Akt at Thr-308 (Fig. 1A).

A DAF2/DA assay revealed that fenofibrate significantly increased the fluorescence levels reflecting NO production in HUVEC, whereas L-NAME reversed them, as expected (Fig. 1C).

Fenofibrate activated AMPK in HUVEC

We further investigated the effects of fenofibrate on AMPK in detail. Treatment of HUVEC with fenofibrate caused an increase in AMPK phosphorylation in a